Mapping undercover: integrated geoscientific interpretation and 3D modelling of a Proterozoic basin.

Mark Lindsay[1], Sandra Occhipinti[1,2], Crystal Laflamme[1,3], Alan Aitken[1], Lara Ramos[1]

5 [1]The Centre for Exploration Targeting, School of Earth Sciences, The University of Western Australia, Crawley, Western Australia, 6009, Australia
[2]Mineral Resources, Commonwealth Science and Industry Research Organisation, Kensington, Western Australia, 6151, Australia
[3]Department of Geology and Geological Engineering, Laval University, Québec, G1V 0A6, Canada

10 *Correspondence to*: Mark D. Lindsay (mark.lindsay@uwa.edu.au; markdlindsay@gmail.com)

Abstract. Gravity and three-dimensional modelling combined with geochemical analysis are used to examine the subsurface within, and below the poorly exposed Paleoproterozoic Yerrida Basin in central Western Australia. Understanding the structure of a region is important as key features indicating past geodynamic processes and tectonic activity can be revealed. However, in stable, post-depositional tectonic settings only the younger sedimentary units tend to be widely exposed

15 rendering direct observation of basement and intrusive rocks impossible. Geophysical imaging and modelling can reveal the structure of a region under cover. High amplitude density anomalies around the basin cannot be reconciled with current geological knowledge in the case presented here. The density anomalies infer an abundance of buried and high-density material that is not indicated by the surface geology. A hypothetical causative source for the high-density anomalies is considered to be intrusion and extrusion of volcanic mafic rocks during rifting of the basin. The simplest and plausible

20 stratigraphic attribution of these interpreted mafic rocks is to the Killara Formation within the Mooloogool Group. However, geochemistry reveals that the Killara Formation is not the only host to mafic rocks within the region. Mafic rocks present in the Juderina Formation have largely been ignored in previous descriptions of Yerrida Basin magmatism and results indicate that they may be far more substantial than once thought. Sulphur isotopic data indicates no Archean signature to the mafic rocks, a somewhat surprising result given the basement to the Basin is Archean Yilgarn Craton. It is proposed the mafic

25 rocks were sourced from vents located to the north along the Goodin Fault or under the Bryah sub-basin and Padbury Basins. The conclusion is that the formation of the Yerrida Basin involves a geodynamic history more complex than previously thought. The utility to the approach described here is examined for application to cratonic sag-basin environments. This result highlights the value in geophysics and geochemistry to reveal complexity in the earlier geodynamic evolution of the basin that may be indiscernible from surface geology, but may have high importance for the tectonic development of the

30 region and its mineral resources.

1 Introduction

The Yerrida Basin presents an opportunity to examine covered geological architecture with a range of geophysical techniques. This opportunity exists because multiple geophysical data are required to delineate anomalies that can be interpreted to be structure, rock bodies or both. That no individual physical field adequately reflects all the elements required

35   to construct a meaningful model stems from the ambiguity of geophysical data (Nettleton, 1942;Fullagar et al., 2004). Different lithologies often share very similar characteristics for a single petrophysical attribute (igneous, metamorphic and sedimentary examples with magnetic susceptibility see Grant (1985) and Clark (1997); for density examples see Manger (1963)). Differentiation between geological units is typically made with less ambiguity using multiple petrophysical attributes. For example Perrouty et al. (2012) and Lindsay et al. (2016) use magnetic susceptibility and density

40   measurements for both structural interpretation and forward modelling to differentiate geological units. This scenario is not unique, and typically any geological investigation using geophysics requires at least two physical fields to reveal architectural elements with less ambiguity to the interpreter (Aitken and Betts, 2009;Blewett et al., 2010;Dufréchou et al., 2014;Lindsay et al., 2016;Perrouty et al., 2012). These examples show how increased interpretation confidence is provided by identifying co-located anomalies present in multiple datasets. The reasoning is that if an anomaly is present in multiple

45   datasets it is less likely that: (i) the anomaly has not been introduced as an artefact during data processing or collection and (ii) it is significant enough that it influences each of the represented physical fields to produce a detectable anomaly.

An alternative and less sceptical viewpoint is to use multiple datasets to detect anomalies because some geology only has a detectable response in specific physical fields, or with certain orientation. For example, gravity and magnetic data were used by Lindsay et al. (2017) to delineate structure from a region in the east Kimberley, northern Western Australia. Recognising

50   that the density and magnetic properties that potential field data provide a restricted image of the crust, magnetotelluric data was included to include distribution of resistive properties which have been used to identify where fluid pathways and mineralised zones exist based the presence of conductive anomalies (Heinson et al., 2006;Dentith et al., 2018). Brethes et al. (2018) use magnetic and electromagnetic data with field observations to perform interpretation of the Jameson Land Basin, Greenland, and Kohanpour et al. (2018) use gravity and magnetic data in combination with numerical modelling to

55   determine the existence and location of deep- and crustal-scale structures. Similar investigations to mafic magmatism have been effectively conducted using geophysical data and modelling. Blaikie et al. (2014) use detailed gravity and magnetic surveys to compare the structure of maars and diatremes in the Newer Volcanics Province (NVP, Victoria, Australia), and infer their eruptive histories. At larger scales, Deng et al. (2017) developed a 3D image of lithospheric density in the Tarim block, central Asia, which is covered by 5-15 km of basin sedimentary rocks. A combination of seismic velocity, gravity

60   topography and crustal thermal models permitted investigation of the history of deformation and related magmatism.

Geochemistry provides valuable insight to the interpretation process through rich characterisation of rocks with multiple elemental attributes. Fundamental differences between rocks and their composition can be identified, and in the case of magmatic rocks, the genesis and source of formation interpreted. Armit et al. (2014) use whole-rock geochemistry to define

65   characteristic rare earth element (REE) geochemical patterns to support their geophysical interpretation of rock types in their reconstruction of the northern Mount Painter Inlier. Perrouty et al. (2017) and Perrouty et al. (2018) use geophysical interpretation to identify dyke swarms in the Canadian Malartic, then use geochemistry to investigate metasomatic footprints for Au mineralisation.

Geological constraint is required to support geophysical interpretation and modelling. The inclusion of field- or core-collected data is arguably the best way to reduce geophysical and petrophysical ambiguity (Betts et al., 2003;Brethes et al.,

70   2018;Perrouty et al., 2012). Husson et al. (2018) use geological measurements and interpretations in the form of a petrophysically attributed 3D geological model to constrain gravity inversion and locate karstified regions in the Languedoc area, southern France. Such regions, covered by large areas of regolith, transported cover or basin sedimentary rocks make opportunities to make relevant observations of the target rare. Mineral explorers will require geophysics to explore effectively, even in areas with sufficient outcrop, as most exploration is now focused on targeting buried mineralisation

75   (Müller and Groves, 2019). Thus a necessary reliance on petrophysical constraint ensues when geophysical interpretation and modelling become the only convenient methods to examine geologic structure.

This paper describes how different data sets were used to identify various parts of basin architecture through structural interpretation, geophysical forward modelling, 3D structural modelling, geophysical inversion and whole rock geochemistry. Structure was interpreted through a combination of magnetic, electromagnetic (EM) and remotely-sensed data and integrated

80   with petrophysical measurements and geological field observations. Geophysical modelling was used to further expand understanding of architecture into three-dimensions. Geochemistry was used to determine whether the interpreted mafic bodies were likely to be the Killara Formation basalts, or different bodies that may be associated with the Juderina Formation. The results were then considered to determine whether and where the Yerrida Basin might be prospective for VMS mineralisation.

85   **2 Yerrida Basin Geology**

The Paleoproterozoic Yerrida Basin is located on the northern margin of the Archean Yilgarn Craton, within the southern part of the Capricorn Orogen (Figure 1) and extends approximately 150 km from north to south, and 180 km from east to west. Other Paleoproterozoic basins are located at the margins to the Yerrida Basin: the Bryah sub-basin and Padbury Basin (north and west) and Earaheedy Basin (east). The Byrah sub-basin was recently found to be a sub-basin of the Yerrida Basin

90   by (Occhipinti et al., 2017). Archean rocks also bound the basin with the northern extent of the Wiluna Greenstone belt to the southeast, and Yilgarn Craton granite-gneiss to the east. The Archean Goodin Inlier sits within the Yerrida Basin. The Archean Marymia Inlier is located to the north and separated from the Yerrida Basin by part of Bryah Basin.

The stratigraphy of the Yerrida Basin, summarised in Figure 2 and by Occhipinti et al. (2017), is comprised of underlying

95   Archean basement of granite-greenstone rocks typical of the Yilgarn Craton. The Wiluna Greenstone Belt is located at the

southeastern edge of and unconformably overlain by the Yerrida Basin. The Merrie Greenstone Belt is located at the eastern edge of the Basin and is unconformably overlain by Yerrida Basin and Earaheedy Basin rocks. The Goodin Inlier is an elliptical, roughly 30 x 45 km fragment of Archean granitic basement unconformably overlain by the Windplain Group, the basal units of the Yerrida Basin. Goodin Inlier rocks are heavily weathered, dominantly monzogranite and mostly

100   undeformed except at its southwestern margin. East to southeasterly trending mafic dykes intrude the Goodin Inlier and are marked in places by sericitised feldspars produced by contact metamorphism (Adamides, 1998). The Marymia Inlier, also an Archean fragment, is located to the north and northeast of the Yerrida Basin and was likely reworked during the Paleoproterozoic (Bagas, 1999). Sedimentation patterns and development of the Yerrida Basin were likely influenced by both the Goodin and Marymia inliers and uplift early in basin development (Pirajno et al., 1998).

105   The development of the Yerrida Basin began with deposition of the c. 2200 Ma Windplain Group, followed by the 2180 to 1996 Ma Mooloogool and Bryah Groups (Occhipinti et al., 2017;Pirajno and Occhipinti, 2000). The rocks of the Windplain Group are representative of a shallow coastal and possible epicontinental setting (Occhipinti et al., 2017), while the rocks of the Bryah and Mooloogool Groups were deposited in relatively higher-energy and possible rift environments (Occhipinti et al., 2017;Pirajno and Adamides, 2000). Periods of magmatism are recorded primarily by the basaltic volcanic and intrusive

110   rocks of the Killara and Narracoota Formations (Mooloogool and Bryah Groups, respectively), though other mafic intrusive and extrusive rocks are observed in other formations (Juderina and Karalundi Formations, Occhipinti et al., 2017) and as dykes (Mueller, 2011). The geodynamic evolution of the Yerrida Basin is interpreted as a pull-apart basin opening consistent with a trailing-edge marginal sag-basin (Pirajno and Occhipinti, 2000), progressing to a rift in the north (Bryah Sub-basin) (Occhipinti et al., 2017;Olierook et al., 2018). Continued extension resulted in the intrusion and extrusion of the Killara

115   Formation tholeiitic basalts (Occhipinti et al., 1997). Basin development ceased with deposition of the Maraloou Formation (Mooloogool Group) shales and siltstones in a lacustrine environment (Pirajno and Adamides, 2000;Pirajno and Occhipinti, 2000;Occhipinti et al., 2017). The Mooloogool Group is unconformably overlain by the Yelma Formation (Tooloo Group) and is the basal unit of the Earaheedy Basin (Occhipinti et al., 2017).

2.1 Mineralisation Potential

120   The Yerrida Basin is host to epigenetic lead-carbonate and oxide mineralisation at the unconformable contact between the carbonate and sandstone rocks of the Juderina Formation and the overlying Yelma Formation (Pirajno and Occhipinti, 2000). Potential for epithermal copper exists in the Thaduna Formation due to the presence of the Thaduna Copper Mine (Pirajno and Adamides, 2000). VHMS mineralisation is exhibited by the DeGrussa Cu-Au-Ag deposit (12.Mt @ 4.7% Cu and 1.8 g/t Au) and is associated with mafic volcanism at 2045 Ma (Hawke et al., 2015). While mineralisation is hosted in the Karalundi

125   Formation of the Bryah Group, the synchronous deposition of the Juderina and Johnson Cairn formations (Occhipinti et al., 2017) has generated interest in the Yerrida Basin for VHMS mineralisation, especially along the northwestern margin and Goodin Fault.

3 Methods and Datasets

3.1 Rock Properties

130   Rock properties measured from samples collected from the study area provide an important constraint for any structural interpretation or modelling of geophysical data (Figure 1). Samples were collected from outcrop and carefully assessed to be free of contamination from weathering and alteration, however it is noted that there is a higher risk of contamination from surface outcrop that drillcore. Magnetic susceptibility and density properties help to guide reasonable discrimination of rock types from magnetic and gravity datasets during interpretation. The rock properties are also used to constrain geophysical

135   ambiguity during forward and inverse modelling in an attempt to ensure that some representation of the target geology is maintained. The rock property data collected from the study area guided the classification of geological units in the structural interpretation and provided the basis of the susceptibility and density values used in forward modelling.

3.2 Potential Field Data

Magnetic data (Figure 3a) was obtained from the Geological Survey of Western Australia in grid form with an 80 m cell size

140   that had been differentially reduced to the pole (dRTP) (Brett, 2013). The resulting dRTP grid is a mosaic of government-funded aeromagnetic surveys with line-spacing between 200 m and 400 m. Various transforms and filters were applied to the dRTP grid to subdue or enhance particular features and included tilt, vertical and horizontal derivatives, analytic signal, upward continuation and dynamic range compression (DRC - see Kovesi et al., 2012 for details).

Bouguer gravity data (Figure 3b) were obtained from the Australian National Database maintained by Geoscience Australia

145   and have been corrected for terrain and spherical-cap effects. Older data from the eastern part of the Capricorn Orogen preserve topographic effects as only the most recently acquired surveys are terrain-corrected. Most gravity data have a station spacing of between two and four km, however in areas of more sparse coverage spacing can be up to 11 km. A grid was interpolated using a minimum curvature algorithm (Briggs, 1974) and used for interpretation and modelling. The gravity grid and variations were produced with a cell size of one km to provide the necessary detail and coverage.

3.3 Structural Interpretation

Aeromagnetic data was used to interpret the upper crust to determine the smaller-scale structural architecture with methods demonstrated by Aitken and Betts (2008), Betts et al. (2007), Gunn (1997) and Lindsay et al. (2017).. Magnetic data was difficult for extracting geological content for three reasons. (1) The basin sedimentary rocks do not display enough magnetic susceptibility contrast to allow discrimination of structure; (2) the basin architecture is mostly flat-lying, thus most rock

155   boundaries (and thus potential locations of high petrophysical contrast) were parallel to the plane of view used during interpretation and; (3) magnetic regolith and stream sediments obscure the underlying structure.

Low-pass and upward continuation processing was used to remove the shorter wavelengths in the magnetic signal in order to lessen the obscuring effect associated with these magnetic cover units. Upward continuation also removed shorter

wavelengths that may have been associated with the bedrock geology, making detailed near-surface structural interpretation

160   more difficult.

The following filters proved the most useful for magnetic data in different areas on the Basin: first vertical derivative (1VD); auto-gain control (AGC); tilt-derivative (TDR) and dynamic range compression (DRC). 'Blending' grids facilitated better resolution of structure, where two grids are overlain, and one is made semi-transparent. This practice was particularly useful with the magnetic data. Bouguer gravity data and its 1VD was used to identify larger structure, and to provide additional

165   insight to regions where magnetic susceptibility contrast was low (Almalki et al., 2015;Fairhead, 1976;Hildenbrand et al., 2000).

Field based geological information was obtained from "WAROX", the Geological Survey of Western Australia (GSWA) rock observation database (Geological Survey of Western Australia, 2018) [44] and used to locate some structures, but was principally employed to understand geometry and orientation of interpreted structures. WAROX data was invaluable for

170   generating a 3D understanding.

3.4   Magnetic and Gravity Forward Modelling

The map interpretation was supported by geophysical forward modelling a section crossing the northwestern part of the Yerrida Basin (Figure 3a and b) to provide an understanding of the basin architecture at depth. The section transects the northwestern edge of the Yerrida Basin, the Goodin Inlier and part of the central part of the Basin. The structure and geology

175   of the surface and upper crust was constrained predominantly by geological observations taken from WAROX and GSWA 1 000 000 and 1:250 000 scale maps (Appendix 1) and our own fieldwork. The petrophysical model generated by forward modelling was constrained with density and magnetic susceptibility data that supported the subsequent geological interpretation. Forward calculation of the geophysical response was undertaken using the GM-SYS application in Geosoft Oasis Montaj® (https://www.geosoft.com/products/oasis-montaj) software following the methods of Talwani et al. (1959).

180   The purpose of forward modelling with this method is hypothesis testing so possible geological scenarios are tested against the observed geophysical data. Scenarios were proposed that explored different dip directions of the Goodin Fault, and the configuration of high density bodies (single or multiple superposed bodies) along the section. The model with the lowest misfit that also plausibly corresponds to the geology is presented in the results section.

3.5 3D Modelling and Geophysical Inversion of Gravity

185   3D modelling was performed using Intrepid Geophysics Geomodeller© (Calcagno et al., 2008). The purpose of producing a model was two-fold: (1) to better understand the 3D architecture of the basin and; (2) test the modelled architecture against the observed regional geophysical response across the entire basin. Geophysical modelling techniques were both 3D forward modelling (Talwani and Heirtzler, 1964;Talwani et al., 1959) and geophysical inversion (Guillen et al., 2008). Geomodeller software allows the stratigraphy to be defined as a topological constraint with interpreted structure deformation assigned to

190   each stratigraphic unit, so that deformation timing can be established and only geological units of equivalent age or older are

affected. As with all 3D modelling packages, some upscaling of data needs to be performed (Lindsay et al., 2012), so only the larger and more significant structures were included. This is because of limitations in the algorithms these packages use in reproducing complex geometries typically encountered in the natural world (Jessell et al., 2014). Stratigraphy was treated similarly, and the modelled units were limited to formations. For example, the Finlayson and Bubble Well members were not

195 modelled individually, but represented by the parent Juderina Formation. Likewise, the 3D modelling algorithm provided by Geomodeller does not allow for joint modelling of more complex geological relationships, such as equivalent facies nor intercalated formations (for example, the Doolgunna and Thaduna formations) (de Kemp et al., 2017). Simplifications are thus required with all formations being represented as discrete units, though still belonging to the same group. The stratigraphic input data are summarised in Figure 2.

200 Geophysical inversion was performed using the 'total litho-inversion' method of Guillen et al. (2008), a stochastic process which obtains a 3D probabilistic description of geological objects while constrained by the available data: geological boundaries (our interpretation), petrophysics (density) and the observed geophysical field (the gravity grid). A range of model geometries and rock property values are tested and returns a model and a probability distribution over model space which addresses issues surrounding deterministic inversion methods of non-uniqueness and attempting to identify the 'best'

205 or 'most probable' model (Tarantola, 2006). The input to inversion is the geological model with petrophysical properties assigned to each formation. Inversion can result in some violations of model topology, where implausible stratigraphic relationships are recovered as they provide a less costly mathematical solution. This method allows constraints to applied to ensure that model topology (i.e. the stratigraphy - Figure 2) was not violated and that recovered lithologies remain in the stratigraphic correct order.

210 **3.6 Geochemistry**

Ultramafic and mafic rock samples obtained from the Yerrida Basin were analysed for major and trace element geochemistry at the commercial ALS laboratory, Perth. Further details (data tables and methods) are provided in the supplementary materials of Olierook et al. (2018).

4 Results

215 **4.1 Petrophysics**

Table 1 shows the measured values of both magnetic susceptibility (in SI$\times 10^{-3}$ units) and density (gms/cm^3) from rocks representative of the Yerrida Basin stratigraphy and input for forward and inverse geophysical modelling. Sample locations are shown in Figure 1. The magnetic susceptibility values show very little variation between rock units. This, combined with the magnitude of error that envelops the range of susceptibility values across the measured rock unit, means that accurately

220 differentiating geological bodies with magnetic data in this location is unlikely. Density petrophysics do show greater variability between rock units with less error meaning that gravity data may be more useful than magnetic data to

differentiate geological bodies during forward modelling, even at a lower resolution when compared to the magnetics data. **Figure 5** shows histogram representation for each unit and **Figure 6** shows the same for density.

4.2 Structural Interpretation

225   Initial structural interpretation (Figure 7a) was completed using gravity data at the basin scale. The most useful combination of images at this stage was a blend of the Bouguer anomaly in colour and the 1VD of the RTP magnetics. Some obvious features are the greenstone belts (Wiluna in the south, and Merrie in the east) characterised by a high magnitude gravity anomaly (Figure 7b), and north-northwest trending strong and linear magnetic anomalies, as shown in the RTP/1VD blended magnetic image (Figure 7c). The Goodin Inlier (Figure 7a) is particularly obvious due to its low gravity signature in contrast

230   to moderate signature surrounding it (Figure 7b). The higher magnitude, moderate gravity signature also appears to be quite extensive, and is observed, in some places, to extend to the basin extent (Figure 3b – white line). This suggests the moderate magnitude anomaly is in response to Yerrida Basin rocks, rather than the lower magnitude response basement, as exemplified by the Goodin Inlier. The Wiluna Greenstone belt is interpreted to extend under the southern edge of the Yerrida Basin (interpreted boundaries indicated by the yellow line in Figure 7b) as its characteristic signature extends almost as far

235   north as latitude 26° south, and dominates the gravity response of the southeastern corner of the basin.

More detailed structural interpretation at 1:100 000 scale relied upon existing GSWA geological maps, the WAROX (GSWA field observation database), magnetic data, orthophotos, digital elevation models, Landsat 8 and ASTER data provided as CSIRO Geoscience products (Cudahy et al., 2008). Gravity data was used where resolution allowed structure to be interpreted. Two stages of interpretation were conducted. First, linear and planar geologic structure such as faults,

240   fractures, dykes and folding was interpreted by using a combination of the available data, then lithology was interpreted (Figure 7a). The two stages were not conducted in isolation, as each stage needed to be consistent with the other to maintain basic geological principles and rules, and thus plausibility.

In both parts of the interpretation, magnetic data proved to be less useful here than other data. The magnetic grids show very little contrast in the Yerrida Basin rocks (Figure 7c), and this is supported by the magnetic susceptibility results shown in

245   **Figure 5**. Some of the interpreted faults are supported by field mapping, the geological maps, and our own field validation (Figure 1– note site locations). Some faults were interpreted from anomalies using a combination of magnetic data processed using dynamic range compression (Kovesi, 2012), auto gain control and the 1VD. Nonetheless, in many cases the suspected location and presence of faults needed to be supported with remotely sensed data, with the DEM being particularly useful. As such, deeper faults with no surface expression may not have been captured in this interpretation, aside from those

250   interpreted from gravity data.

Lithological interpretation relied more heavily on datasets other than potential fields. Typically, lithologies can be discriminated successfully by observing textural differences in magnetic data, with variations in amplitude, frequency and orientation given particular lithologies as characteristic signature (Aitken and Betts, 2009;Betts et al., 2004;Lindsay et al., 2016;Perrouty et al., 2012) . The RTP data shows near-surface anomalies interpreted to be surface processes such as stream

255   and channel sediments and magnetic regolith (for example Fe and/or Mg-rich lag) (Figure 4 – circled in red). Upward continuation was used to filter out these effects by attenuating the shortest wavelengths in the data.

Remotely-sensed data was more useful for interpretation, but used with caution as regolith in the Yerrida Basin is widespread and covered any basin rocks that could be interpreted from satellite data. The widespread extent of regolith was confirmed by our own field observations. Airborne electromagnetic (AEM) data was helpful here, and showed that in some

260   cases bedrock geological could be inferred from what is interpreted to be in-situ regolith (Figure 8a).

The interpretation (Figure 7a) shows an overall E-W, or WNW-ESE orientation of structure in the west and centre of the basin. Structure in the east and southern part of the basin show an orientation of mainly NNW-SSE, similar to the orientation of the underlying Archean greenstone belt and suggests inherited structure from the basement into the basin. The lithological interpretation differs little from existing 1:100 000k and 1:250 000k GSWA maps, and shows that the Juderina Formation

265   forms the base to much of, if not all, the Basin. The Johnson Cairn Formation is less extensive at the surface and is restricted to the western parts of the Basin. Some outcrop in the east suggests the Johnson Cairn may extend under the overlying Mooloogool Group rocks from west to east. A lack of outcrop of interpreted Johnson Cairn Formation in the south suggests it does not extend far to the south, if at all.

Mooloogool Group rocks are interpreted to be located in the central, west, east and northern parts of the Basin, with the

270   youngest rocks of the Maraloou Formation being the southern-most. The tholeiitic basalts of the Killara Formation are most extensive in the east, with some outcrop in the central, northern and western parts. This was unexpected, as the initial interpretation of the gravity data showed a moderate magnitude anomaly to be extensive everywhere in the basin (Figure 7b), and was initially assumed to be the Killara Formation due to the higher density of mafic rocks relative to the basin sedimentary rocks. Thus the initial interpretation of the Killara Formation shown in Figure 7a may not adequately represent

275   its true extent. If the higher density anomaly observed throughout the Yerrida Basin is caused by the Killara Formation, then the extent of this formation needs to be far more extensive. The next sections describe forward modelling and inversion that attempt to falsify this hypothesis.

4.3 Forward Modelling

Petrophysically constrained forward modelling of geophysical data was conducted to test the hypothesis that the Killara

280   Formation is more extensive undercover than was shown through interpretation. Three stages of forward modelling were conducted: (1) a 3D conceptual study to validate our primary assumptions; (2) 2D section modelling of geophysical data with geological constraints and; (3) forward modelling of a 3D geological model.

4.4 Conceptual Modelling: Noddy

'Noddy' is a kinematic modelling package that allows input of geological events and stratigraphy to generate a 3D model of

285   the resulting architecture (Jessell, 1981;Jessell and Valenta, 1996). A useful part of Noddy is being able to generate the potential field forward response of the model. By assigning petrophysical values to each stratigraphic layer in the model, a

representative grid of the model can be generated (the 'calculated response') and compared to that provided by the geophysical survey (the 'observed response' – Figure 9a and b). Figure 9c shows the basement configuration of the conceptual model with the assigned petrophysical attributes. Yerrida Basin (not shown in Figure 9c) is thus assumed to have

290   Archean basement, with the exposed Goodin Inlier forming a dome.

Three geological scenarios were explored (Figure 10). The first simulates that no Killara Formation is present to explore what the geophysical response would be if there was very little, or no high-density material in the Basin (Figure 10a). The second simulates a 500 m thick layer of high-density material representing the Killara Formation in stratigraphic position

295   (Figure 2) between the Maraloou and Doolgunna formations (Figure 10b). The third simulates 2000 m of high-density material (Killara Formation) in stratigraphic position (Figure 10c). The resulting gravity grids are shown in greyscale with the corresponding model, and profiles (A – A') sampled from the gravity grids.

300   Having no dense material in the basin (Figure 10a) clearly does not recreate the observed gravity response with the Goodin Inlier producing a gravity high, rather than the low as shown in the observed response (Figure 9b). Adding 500 m of dense material (Figure 10b) produces a marginally closer fit to the observed response, but the Goodin Inlier still produces a gravity high, though with a lower difference (8.7 mGal) than in the previous example (15.7 mGal). Adding 2000 m of dense material does produce a response that shows the Goodin Inlier to produce a gravity low, and somewhat similar to the observed

305   response. However, this calls for the Killara Formation to be consistently 2000 m thick, which is twice as much as the 1000 m formation thickness estimated from previous work (Pirajno and Adamides, 2000).
The results from conceptual modelling with Noddy support the hypothesis that a significant amount of dense material in the basin can produce the gravity response seen in the observed data. However, the reality is almost certainly more complex than a single, horizontal and lithologically homogenous layer. The dense material is likely to be a combination of widespread

310   Killara Formation and sills or possibly intrusions produced through related magmatism.

4.5 Testing Intrusive Scenarios with 2D geophysical forward modelling

Geosoft® GM-SYS is a forward modelling platform that allows easy exploration of geologically complex scenarios (Talwani and Heirtzler, 1964;Talwani et al., 1959). A profile was selected that extended from the northern edge of the basin to the southeast, across the Goodin Fault, the Goodin Inlier and into the centre of the basin (Figure 3) and in similar location

315   to the profiles produced in Noddy (Figure 9a). The same hypothesis is being tested: whether the dense material, possibly the Killara Formation and its intrusive components can account for the gravitational response in this region, however this form of forward modelling allows for more complex geometries to be tested manually.
A selection of plausible models were generated in accord with the geologic history of the region. The main questions were:

(1) how sensitive is the gravity response to the dip-direction of the Goodin Fault? This was tested by changing the dip

320   direction from the northwest, to sub-vertical, and to the southeast.

(2) what configuration of high density bodies are required. Two scenarios were examine, one where the high density

     bodies were assumed to be extrusive mafic lavas associated with the Killara Formation, thus no intrusive

     component. The other was that multiple superposed bodies were possible, so assuming both intrusive and extrusive

     modes of magmatism.

325   Five scenarios were generated from these assumptions. Figure 11 shows the model which is the most consistent with the geological interpretation (Figure 7), geological observation (Table A1) and the potential geophysical data (Figure 3). Figure 11a and b show both the magnetic and gravity (respectively) observed response (dots) and the calculated response (line). The calculated response is produced from the geological section (Figure 11c), where petrophysical values are assigned according to values measured from the field. The geological section was constructed using geological observations taken from GSWA

330   maps and WAROX (Appendix 1), and integrated into the model so that existing structural relationships are maintained, and general geological reasoning is not violated.

     The model fits well to both the magnetic and gravity data. Geological interpretation (Figure 11d) of the petrophysical model (Figure 11c) shows that the Killara Formation has been successfully modelled as a set of faulted sills. This supports the hypothesis that the Killara Formation may be the source of the moderately high gravity anomaly throughout the Yerrida

335   Basin. This interpretation of sills and intrusion is consistent with that of Pirajno and Occhipinti (2000).

     At the northwestern end of the section (left-hand side of Figure 11d), the boundary between the Yerrida Basin rocks (Doolgunna and Juderina formations) and the Byrah Basin rocks (Karalundi Formation) has a distinctive signature, especially in the magnetic data (Figure 11a). The geological model shows a very steep dip to the northwest (or left-hand side of the section) and a possible downward throw as indicated by the footwall Yilgarn Craton modelled on the Yerrida Basin

340   side of the boundary. The Goodin Fault has been suggested to be at this location, and this model shows it to be a normal, northwest dipping fault, in contrast to the northwest dipping thrust structure reported by Pirajno and Adamides (2000) but consistent with the interpretation of Occhipinti et al. (2017). The analysis presented here is certainly not conclusive, and the presence of the Goodin Fault is still under question, as are its characteristics.

4.6 3D Model

345   The hypothesis of mafic rocks attributed to the Killara Formation are the causative source of the gravity anomaly throughout the basin now appears feasible. Hypothesis testing on simple models and a section around the Goodin Inlier provide some support, but whether this relationship is consistent for the entire basin also needs to be tested. Modelling was expanded to include the entire basin in 3D to achieve these aims.

A 3D model was constructed using Geomodeller, an implicit modelling platform that allows models to be constrained by
350 known stratigraphy, fault relationships and geological observations (Calcagno et al., 2008). Geomodeller also offers
geophysical modelling tools, including forward modelling and inversion (Guillen et al., 2008), which operate directly on the
3D geological model.

Data input to the model was gathered from the stratigraphy (Figure 2) and structural interpretation (Figure 7a, Figure 11d).
However, only the larger faults were retained for 3D modelling, as the smaller, more insignificant faults degrade
355 performance of the modelling engine without providing a commensurate increase in geological understanding to this study.
Each geological unit constructed in the 3D model has petrophysical values (**Figure 5**, **Figure 6**) assigned to allow a forward
response to be calculated.

The 3D model contains what were considered to be important components to produce a representative geophysical response:
the Goodin Inlier; Archean basement; Yerrida Basin sedimentary rocks; the Wiluna and Merrie greenstone belts and various
360 faults, including the north-northwest-ward extension of the Ida Fault (Figure 12). It is important to note the northwestern
corner of the model, where the Bryah-Padbury basin would be, is not included in the modelling. The focus of this study is on
the Proterozoic basin rocks rather than the Archean basement as Giraud et al. (2019) described in a comprehensive analysis
of the underlying greenstone belts using sophisticated inversion techniques constrained by uncertainty.

4.7 3D Forward Modelling and Inversion.

365 3D forward modelling was performed to investigate the density structure of the Yerrida Basin. Initial attempts at modelling
the gravity produced similar results to those shown in the conceptual stage (Figure 10b and b). Including the Killara
Formation as a thin unit showed that this had almost no effect in producing a gravitational anomaly (Figure 10b). Learning
from this result guided the construction of the 3D geological model to include a more substantial component to the Killara
Formation. The modelled intrusive bodies were quite thick (=>1000m) and extensive but were still not sufficient to replicate
370 the observed signal. Evidentially an additional source of high-density material needed to be considered.

4.8 Juderina Formation and a Substantial Mafic Component.

Drill core from a range of diamond-drilled boreholes (THD1, DGDD347, DGDD020, DGDD278, DGDD279, DGDD281,
DGDD319, DGDD320, DGDD404, DGDD406 and THDD 226) reveal that the Juderina Formation contains mafic sills,
either as finer-grained basaltic, or micro-gabbroic rocks at depth. This observation is particular to the Juderina Formation,
375 and not the overlying Johnson Cairn, Thaduna, Doolgunna and Maraloou formations. Reasoning suggests that the mafic
component of the Juderina Formation was intruded during or soon after deposition of the clastic and carbonate component of
the formation, and was thus restricted to just this formation. Another option is that the mafic component to the Juderina
Formation is related to the intrusive parts of the Killara, Karalundi or Narracoota formations, however if this was true,
formations underlying the extrusive Killara Formation component (Johnson Cairn, Thaduna and Doolgunna formations)
380 should also contain some proportion of mafic intrusive rocks, which (to our knowledge) they do not. Thus, adding higher

density bodies proximal to or within the Juderina Formation is a reasonable means to reproduce the anomalous gravity signature.

Geophysical inversion provides a means to test the hypothesis that higher density rocks can explain the anomalous density signature. An incremental approach, similar to that with the simplified models (Figure 10) was taken to ensure that multiple

385 scenarios are considered while simultaneously performing sensitivity analysis. The following scenarios were tested:

1. No additional high density intrusions are modelled – only the Killara Formation rocks are high density (>3.0 gm/cm^3)

2. A moderate increase in the volume of high density intrusions in locations suggested by the section-based forward model (Figure 11)

390
3. A large increase in the volume of high-density intrusions, as guided by the location of high-density anomalies in the observed gravity data (Figure 3b).

Inversion was conducted by discretising the geological model into cells of 2000m x 2000m x 500 m (x, y and depth axes respectively). The maximum number of iterations was to 1M but was exceeded before convergence was achieved. The 'success' of the inversion was judged on global statistics (RMS misfit) and locally, by investigating how inversion produced

395 the necessary density structure to reproduce the observed gravity field at specific locations.

Each inversion was executed to allow the contacts of the Juderina Formation, intrusive bodies and the Archean greenstone units to move if required by the inversion. All other units were left fixed. These constraints reflect our knowledge of which rock units contain high-density rocks, and whether changing the geometry or petrophysical properties of these particular rocks can explain the density structure of the Yerrida Basin.

400 All scenarios were successfully inverted and produced a root-mean-square (RMS) misfit of approximately 4 mGal from an initial misfit of over 20 mGal, with the final misfit values (Figure 13) and convergence curves almost identical. While a 'successful' inversion and corresponding reduction of RMS misfit by 80% is satisfactory, the almost identical convergence curves and final values alone are inadequate as indicators of geological plausibility. Deeper geological analysis of the resulting model is needed. Results are shown in Figure 13. The upper panel of part (a) shows the geological model, the

405 middle panel shows the observed gravity data that was input and the lower panel shows the prior model extents of the Wiluna and Merrie greenstone belts ('W' and 'M' respectively). Part (b), (c) and (d) top panels show the geological prior model used for input (scenarios 1, 2 and 3 respectively) with only the included mafic intrusions displayed for ease of visualisation. The middle panels of (b), (c) and (d) show the gravity field calculated from the inverted model. A minimum threshold of 2.9 gm/cm^3 was chosen as only mafic rocks are generally expected to show density higher than this (Telford et

410 al., 1990). Another plausible possible source of higher density material in this region is dolomite, however these are unlikely to have densities >2.9 gm/cm^3 (Telford et al., 1990). The lower panels of Figure 13 shows the distribution of locations

determined by the inversion to be > 2.9 gm/cm^3 density and possible mafic bodies. A discussion whether dolomite or basalt is more plausible is conducted in the next section.

The middle panels of Figure 13 highlight two regions that are investigated in more detail: '1' – in the west; and '2', in the
415   centre of the Yerrida Basin.

Region 1: The observed gravity data shows a high magnitude anomaly in Region 1. The lower panels in Figure 13 show that the inversion requires dense material >2.9 gm/cm^3 to be placed here to account for the anomaly in the observed data (Figure 13a middle panel), regardless of the geological prior model used for input. Scenarios 1 and 2 do not have mafic bodies modelled in this location (see upper panels), so rocks within the Juderina Formation exhibit densities at >2.9 gm/cm^3 in these
420   inversion results from these scenarios. Scenario 3 includes a mafic body in this location (Figure 13d – top panel) and the inversion includes higher density material in this location as well, but more laterally extensive than in scenarios 1 and 2.

Region 2: The observed gravity data shows a higher amplitude gravity anomaly in this location (Figure 13a – middle panel). To the east, the deeper presence of the northern extension of the mafic component of the Wiluna Greenstone Belt (WGB) is interpreted to be the causative body of the higher magnitude gravity values (Figure 13a bottom – 'W'). The western edge of
425   the high amplitude region also displays a high amplitude anomaly, though of lesser magnitude than the WGB (Figure 13a-d - white box). Scenarios 1 and 2 show that this part of the model is not adequately resolved through inversion, while Scenario 3 shows some improvement, though not enough to explain the southerly portion of the anomaly. A zoomed comparison is shown in middle panel inset of Figure 13a (observed field) and Figure 13d (inverted model): the asterisk indicates where additional higher density material is needed to be for a better fit to the observed field.

430   Scenario 3 has been judged the best to represent the geological structure of the basin that best reproduces the gravity signature of the Yerrida Basin. Some issues remain with the model as shown in Figure 14.

5 Discussion

The process of collating, interpreting and modelling geoscientific data leads to a greater understanding of the capabilities of the available data. This expands the existing knowledge of the target region which can then inform decisions for future data
435   collection, interpretation and modelling. The geoscientist performing these exercises gains all this knowledge, but whether this knowledge can then be effectively communicated so other benefit is challenging (Quigley et al., 2019). The discussion that follows attempts to do this by first presenting a range of outcomes that were considered useful. Some of these outcomes are not 'successful' in the traditional sense, but nonetheless are worthwhile reporting, in particular which datasets were useful for different purposes, where limitations exist, and what aspects of the range of modelling procedures nonetheless
440   provided useful insight. The second part of the discussion is a synthesis of what was learned about the structure of the Yerrida Basin and potential for mineralisation.

5.1 Alternative for Higher Density Material

The structural and lithological interpretation, augmented by existing GSWA mapping (WAROX) and field validation provided input to the 3D model. The central aim was to determine if the characteristic density signature of the Yerrida Basin

445   was due to more extensive mafic rocks at depth or some other geological reason. An alternative already briefly introduced considered that later diagenetic or near-surface alteration caused this increase in density. Dolomitsation of carbonate rocks forms dolostone when calcite ions are replaced by magnesium ions. Calcite (mean density = 2.71 gm/cm^3) is less dense than dolomite (mean density = 2.84 gm/cm^3), thus dolomitisation is expected to increase the density of a rock. The magnitude of density increase depends on the carbonate proportion of the original rock (with lower proportions resulting in less carbonate

450   to dolomitise, and thus a smaller density increase) combined with the degree that dolomitisation has occurred.

3D geophysical inversion was employed to explore both these scenarios, and the recovered density distribution leads us to which is more plausible. Region 1 required a significant increase in density when compared to the prior geological model to account for the density anomalies seen in the observed gravity data (Figure 13b-d – middle panels). The Juderina Formation forms a significant unit in this area, both in outcrop and at depth and is likely to contain dolomitic rocks. The carbonate

455   portion of the Juderina Formation includes the relatively minor Bubble Well member and is not considered large enough (Occhipinti et al., 2017) to account for the gravity anomaly. In addition, the magnitude of densities required to produce the required anomaly (>2.9 gms/cm^3) is higher than is realistic for dolostone, even if the rock was made entirely of dolomite. Thus, an extensive mafic component in the subsurface is a more likely source of the gravity anomaly in this location. Modelling in region 2 (Figure 13b-d – middle panels; Figure 13a, b) also supports this reasoning, with a large high density

460   (>2.9 gms/cm^3) body required to account for the observed gravity data. Here, the Juderina Formation is not as extensive as in region 1, and the position of the recovered density anomaly implies a closer spatial association with the Killara Formation.

5.2 Density Distribution and Geological Implications

The distribution of mafic units in the Yerrida Basin was determined through geological modelling combined with petrophysically constrained gravity inversion. The distribution of these mafic units determined from modelling is shown in

465   Figure 15, along with the extents of mapped and interpreted Killara Formation for comparison. Also shown are regions 1 and 2 from Figure 13, and two new regions, region 3, defined by the area of misfit (Figure 14) and region 4, which will be discussed later in this section. The grey regions indicate our current knowledge of the extent of the Killara Formation as shown on GSWA maps and geophysical interpretation and can be assumed to only represent outcrop or near-surface (<50m below depth below surface) rocks. The coloured cells are outputs from the final inversion voxet, and represent the predicted

470   extents of mafic material at the surface and at depth. The plan view shows a significant increase in the extent of mafic material from our current understanding. Region 4 is an extensive northeast-trending body of mafic material modelled as Killara Formation.

A series of 3D isom trio views both above and below the geological model as determined by inversion are shown in Figure 16. These views are all from the southwest and show the depth extent of inverted geological units. Of note are the mafic units as depicted in the right-hand panels. The panels on the right show the distribution of mafic material, with the other units (sedimentary, granite-gneiss and greenstones) filtered out to allow better visualisation. The mafic bodies were modelled individually and coloured-coded to differentiate those that were progressively added during scenario testing. The different colours are not intended to indicate that any particular unit is unique in stratigraphic position or composition.

Most of the higher density, mafic material is located close to the surface. The mafic material in region 4 is shown to extend deeper in the southwest part (Figure 16d). This interpretation is consistent with the gravity modelling and interpretation of Hackney (2004), who suggests the Yerrida Basin deepens and extends under the Byrah-Padbury Basin to the north. Here the higher density material could be part of the Killara Formation, or a substantial part of the mafic component to the Juderina Formation. Figure 16b – 'A' also shows the Juderina Formation is very thick (>10km, and up to 20km) and deepens towards the northeast. Twenty kilometres is almost certainly too thick and is likely due to a combination of artefacts resulting from inversion and the presence of thick (~7km) and dense Narracoota Formation rocks (Pirajno et al., 1998) hosted in the hanging wall of the Goodin Fault to the northwest. Nonetheless, it indicates that a thicker portion of the Yerrida Basin exists here, just that the thickness is difficult to determine.

5.3 Distinguishing Mafic Rocks Using Chemical Composition

Geophysical inversion has been useful in revising the extent of mafic rocks in the Yerrida Basin. What geophysics cannot do with our current dataset is determine whether the interpreted mafic rocks all belong to the Killara Formation, or whether the mafic rocks have different compositions and thus reveal a more complex stratigraphy. The major and trace chemical composition of whole rock samples has been obtained from drillcore (THD001, DGDD347 and the GSWA Geochemistry Database "WACHEM"), surface samples (UWA field work and WACHEM) with analysis and compilation by Olierook et al. (2018) to help us achieve this aim.

As DGDD347 is close to the northern boundary of the Yerrida Basin (Figure 1), we check whether any of the mafic rocks sampled in the Juderina Formation are sills or dykes related to the Narracoota Formation. Figure 17a shows the geochemical distribution of mafic rocks sampled from the Yerrida and Byrah-Padbury basins on a basaltic Th/Yb vs Nb/Yb diagram (Pearce, 2014). This type of diagram is usually used to recognise sources of magma to provide insight into the tectonic setting that generated them, with higher Th/Yb representing lavas modified by subduction-related processes, and those with higher Nb/Yb showing increasing levels of crustal contamination. While possible, interpreting such settings from these results is speculative as more detailed stratigraphic and volcanologic work would be required for support. Nonetheless, the diagram proves useful in discriminating between different types of mafic rocks in the region that may have formed at different times and/or in different tectonic settings.

Samples from drillhole DDGD347 ("DG") and TH D001 ("THD") are clustered toward the higher end of both ratios. Most of the DG and THD samples are close to, but not within, the mid-ocean ridge basalt-ocean-island basalt (MORB-OIB) array.

Importantly, the DG and THD samples are distinctive in their tight clustering and position with respect to the Narracoota and Killara formation samples (Olierook et al., 2018), meaning they are different geochemically, and were thus likely generated in a different setting. This interpretation is supported by Figure 17b, a similar diagram to Figure 17a, but uses a TiO₂/Yb ratio on the y-axis as a proxy for deep melting (Pearce, 2008). Here, the DG and THD samples are distinguishable from the

510   Killara and Narracoota formations based on both the TiO₂/Yb and Nb/Yb ratios. DG and THD can also be separated into their own classifications. The DG samples fall within the alkali classification, while the THD samples are mostly classified as tholeiitic basalts. The DG and THD samples have a deep melting signature, whereas most of the Killara and Narracoota samples have a shallow melting signature.

The overall non-arc melting signature of Figure 17b is similar to the interpretation of Olierook et al. (2018) that mafic

515   magmatism in the southern Capricorn region was interpreted to be generated in an intracontinental rift setting. Our results show that the while the larger tectonic setting may not have changed, the magmatic history of the southern Capricorn is likely more protracted, complex and punctuated by periods of mafic magmatism with a changing source (Occhipinti et al., 2017;Occhipinti et al., 1997;Pirajno and Occhipinti, 2000).

5.4 Yerrida Basin Mineralisation

520   Geochemistry can provide insight to the prospectivity of mafic rocks for VMS mineralisation. Flat REE profiles are typical for VMS prospectivity (Hawke, 2016;Hawke et al., 2015) however, both spider diagrams for THD and DG show inclined, and thus VMS-unprospective REE profiles (Figure 18). These observations are also made by Mueller (2011) for drill hole THD001. An example of a flat REE pattern from basaltic and micro-gabbroic rocks sampled from the Degrussa mine are shown in grey for reference (Hawke, 2016).

525   **5.5 Basin Development**

The location of the thicker mafic and sedimentary portion of the basin is juxtaposed against the Goodin Fault. The thicker part of the Yerrida Basin may then represent a deepening of the basin toward the northwest, which occurred during c. 2200 – c. 2000 Ma lithospheric extension and rifting (Occhipinti et al., 2017;Pirajno and Adamides, 2000;Pirajno and Occhipinti, 2000). The mafic component of rifting may have manifested in two forms. Extensive magmatism contemporaneous with the

530   deposition of: (1) the Juderina Formation or (2) the Killara Formation during development of the Mooloogool Group.
A period of extensive mafic volcanism at c. 2045 Ma saw mafic rocks of the Narracoota Formation intrude and overly the Karalundi Formation in the Bryah Sub-basin located to the north and northwest of our study area (Hawke et al., 2015). Occhipinti et al. (2017) suggest that the Killara and Narracoota formations are manifestations of magmatism during rifting in different basin depocentres that temporally overlap. This is supported by Pirajno and Adamides (2000) who interpret the

535   Killara Formation as basalts extruded in a continental setting, with geochemical affinities similar to the hyloclastites of the Narracoota Formation. Gravity modelling performed and interpreted by Pirajno and Occhipinti (1998) who find the Narracoota Formation thickens up to seven km toward the south of the Goodin Fault. If the high density material modelled

here is part of the Killara Formation, then thickening of the mafic Narracoota Formation toward the south, and thickening of the Killara Formation toward the northwest supports the suggestion of Occhipinti et al. (2017) that the current position of

540 Goodin Fault may represent a rift axis and volcanic vent for this period of magmatism.

Regions 1, 2 and 3 identified from the modelled high-density material are thick and suggest additional sites that may represent vents and the source of mafic volcanism (Figure 13b and d). Region 1 is primarily hosted within Juderina Formation and may represent the mafic component. Regions 2 and 3 are hosted within the Mooloogool Group rocks and may be more likely to be composed of Killara Formation. The thickness of the basin around Regions 2 and 3 is modelled to be

545 thicker than elsewhere, and may represent another rift, smaller than the one centred on the Goodin Fault. The substantial high-density material modelled here suggests Regions 2 and 3 are the location of mafic magmatism and a vent, rather than simply a paleotopographic low, in which sedimentary and mafic material with provenance from elsewhere was deposited.

Multiple sulphur isotopic analysis (LaFlamme et al., In review;LaFlamme et al., 2018) show that the Yerrida Basin mafic volcanic rocks have a slight negative Δ33S signature, typical of Paleoproterozoic basins (Johnston et al., 2006). It suggests

550 that these magmas have not interacted with the Archean basement during volcanism. Given the proximity of Archean basement to these rocks, this is somewhat enigmatic and further suggests that magmas were sourced from the deeper parts of the basin. This source region is likely to the north and northwest of the Yerrida Basin where Archean basement (i.e. Yilgarn Craton) is likely absent, or along the Goodin Fault (Figure 19). Yerrida Basin magmatism was likely contemporaneous with that related to Narracoota Formation (Pirajno and Occhipinti, 2000) albeit via different vents (Occhipinti et al., 2017).

555 Figure 19 shows the proposed locations of vents, broadly estimated based on the gravity anomaly and away from Archean rocks. Higher amplitude gravity anomalies are typically associated with locations proximal to vents due to the greater amounts of high-density material, while the vents themselves exhibit a lower magnitude anomaly due to the lack of high-density material around the crater (Blaikie et al., 2014;Blaikie et al., 2012). The gravity signature is unlikely to reveal short wavelengths that would indicate this geometry at the scale of this study, due to both data resolution and burial of these vents

560 under the Padbury Basin, thus vent location is likely to be in areas of higher overall gravity anomaly.

Transport of magmas would likely have occurred along major structures (e.g. the Goodin Fault) or as sills along rock unit contacts. These near-surface magmatic pathways would have transported material around the Archean Goodin and Marymia inliers. Given the supposition that sill intrusion is restricted to the Juderina Formation, it is suggested that the Juderina Formation also extends to the northwest beyond the current extents of the Yerrida Basin Figure 19a and b. This reasoning

565 supports the interpretation of Occhipinti et al. (2017) that the Yerrida Basin underlies the current day location of the Bryah sub-basin and Padbury Basin.

5.6 Application to Other Regions

The approach described in this paper can be applied to other rift-basin regions located on the margins of cratons that host cryptic geophysical anomalies. The Volta Basin is such an example, where rifts have been interpreted from gravity and

570 magnetic data and density anomalies suggest in-fill from mafic volcanics (Reichelt, 1971;Álvaro and Vizcaïno, 2012),

however their three-dimensional distribution and plausibility of the interpretation is not well understood (Jessell et al., 2016). Likewise, the structure of South American cratonic basins remains cryptic (Braitenberg et al., 2007), though recent studies modelling gravity data have shown progress in gaining geological understanding in these regions (Sanchez-Rojas and Palma, 2014).

575 **6 Conclusions**

A comprehensive structural and geophysical study of the Yerrida Basin, southern Capricorn Orogen was completed. A variety of geophysical, geological and geochemical datasets has been used to achieve a better understanding of basin architecture and magmatic history. Structural interpretation with magnetic data was hindered by low- to no-contrast susceptibility and flat-lying geology; however, the AEM data provided by the Capricorn TEMPEST Geophysical Survey

580 gave critical support to lithological interpretation.

A widespread gravity anomaly spatially associated with sedimentary basin rocks was investigated to infer that a considerable high-density component was required that was incompatible with known exposure of high-density rocks and stratigraphic understanding. The hypothesis that the higher density anomaly may be linked to mafic rock bodies was investigated using a set of forward modelling and inversion techniques. First, a conceptual 3D model around the Goodin Inlier was constructed in

585 a kinematic modelling package to evaluate whether a higher density component was required to recreate the observed gravity response. 3D forward modelling showed that layer of mafic material up a 2000 m thick is required to produce a similar response to the observed response. These results were encouraging but deemed too simple to adequately test the likely more complex architecture the gravity data represented.

2D section forward modelling was then used to investigate a transect across the Goodin Inlier to test whether intrusions

590 associated with the Killara Formation (such as dykes and sills) were plausible candidates to produce the necessary gravity response. This was confirmed as plausible, so a basin-scale 3D model was constructed as a prior model for inversion to test where other high-density bodies were throughout the rest of the basin. Gravity inversions were conducted that progressively added mafic bodies to systematically understand the sensitivity of misfit to the observed gravity and increased volume of higher density bodies. Thus our results show that the mafic composition of the Yerrida Basin is likely to be significantly

595 larger than is shown on current maps and represented by the published stratigraphy.

Geochemistry was used to analyse whether mafic units logged in the Juderina Formation from drillcore were the intrusive part of the Killara Formation, which they are not. A localised different set of mafic bodies was revealed suggesting substantial mafic activity associated with the Juderina Formation that does not contain an Archean signature. The proximity of Archean basement suggests that the source of magmatism was not in the basin itself, but at the northern edge either under

600 the Bryah sub-basin and Padbury Basin, or along large structures such as the Goodin Fault.

7 Appendices

Table A 1. Geological data that aided construction of the forward model shown in Figure 11. SOP = Start-of-profile.

Distance SOP m	Structure	Name	Rock W	Rock E
0	*SOP*			
550	Fault	Jenkin Fault	Narracoota	Karalundi
1600	Fault	Murchison Fault	Karalundi	Karalundi
6600	Fault	Goodin Fault	Karalundi	Doolgunna
8150	Contact		Doolgunna	Mt Leake
10350	Contact		Mt Leake	Doolgunna
11100	Contact		Doolgunna	Johnson Cairn
11750	Fault		Johnson Cairn	Johnson Cairn
13150	Fault		Johnson Cairn	Johnson Cairn
13250	Contact		Johnson Cairn	Juderina
13550	Contact		Juderina	Johnson Cairn
14150	Fault		Johnson Cairn	Johnson Cairn
18600	Fault		Johnson Cairn	Johnson Cairn
21900	Contact		Johnson Cairn	Juderina
23000	Contact		Juderina	Goodin Inlier
25000	Fault		Goodin Inlier	Goodin Inlier
25500	Fault		Goodin Inlier	Goodin Inlier
26150	Fault		Goodin Inlier	Goodin Inlier
32000	Fault		Goodin Inlier	Goodin Inlier
32250	Fault		Goodin Inlier	Goodin Inlier
33750	Fault		Goodin Inlier	Goodin Inlier
40550	Contact		Goodin Inlier	Juderina (mag)
41800	Contact		Juderina (mag)	Johnson Cairn
45500	Fault		Johnson Cairn	Johnson Cairn
45800	Contact		Johnson Cairn	Doolgunna
50000	Fault		Doolgunna	Doolgunna
53300	Contact		Doolgunna	Killara
53800	Contact		Killara	Doolgunna
55000	*EOP*			

8 Data Availability

605 **8.1 3D models**

The Yerrida Basin model is supplied in Geomodeller format and available from DOI: 10.5281/zenodo.3245772.

8.2 Noddy

Noddy software, models and their gravity forward response are provided in native format from DOI: 10.5281/zenodo.3245788. A download for Windows installation of Noddy is available from http://tectonique.net/noddy/.

610 ### 9 Author Contribution

ML performed the data compilation, modelling, analyses, interpretation and manuscript preparation. SO contributed to analyses, geological background and interpretations. CL contributed to geochemical data compilation, analyses and interpretation. AA assisted with geophysical data compilation, preparation and interpretation. LR performed the petrophysical analyses and data compliation. All authors contributed to manuscript drafting.

615 ### 10 Competing Interests

The authors declare that they have no conflict of interest.

11 Acknowledgements

MDL thanks the Geological Survey of Western Australia, the Minerals Research Institute of Western Australia and the Australian Research Council (DE190100431) for their support. Thank you to Paul Hilliard (Sandfire Resources) for his 620 invitation to the DeGrussa mine, valuable discussion and supply of geochemical data. Thank you to Camilla Sørensen and Tim Munday (CSIRO) for their assistance with AEM data and imaging (AEM section Figure 8a). Petrophysical analysis was performed in the UWA petrophysics lab with thanks to Cam Adams. Funding for this work was from a West Australian Government Exploration Incentive Scheme grant awarded to UWA from the Geological Survey of Western Australia and the 'Distal Footprints of Giant Ore Systems - UNCOVER Australia', CSIRO Science & Industry Endowment Fund (SIEF).

625 ### 12 References

Aitken, A. R. A., and Betts, P. G.: High-resolution aeromagnetic data over central Australia assist Grenville-era (1300 Ma-1100 Ma) Rodinia reconstructions, Geophys. Res. Lett., 35, 2008.

Aitken, A. R. A., and Betts, P. G.: Multi-scale integrated structural and aeromagnetic analysis to guide tectonic models: An example from the eastern Musgrave Province, Central Australia, Tectonophysics, 476, 418-435, 2009.

630 Almalki, K. A., Ailleres, L., Betts, P. G., and Bantan, R. A.: Evidence for and relationship between recent distributed extension and halokinesis in the Farasan Islands, southern Red Sea, Saudi Arabia, Arabian Journal of Geosciences, 8, 8753-8766, 10.1007/s12517-015-1792-9, 2015.

Álvaro, J. J., and Vizcaïno, D.: Proterozoic microbial reef complexes and associated hydrothermal mineralizations in the Banfora Cliffs, Burkina Faso, Sedimentary Geology, 263-264, 144-156, 2012.

635   Armit, R. J., Betts, P. G., Schaefer, B. F., Pankhurst, M. J., and Giles, D.: Provenance of the Early Mesoproterozoic Radium Creek Group in the northern Mount Painter Inlier: Correlating isotopic signatures to inform tectonic reconstructions, Precambrian Research, 243, 63-87, https://doi.org/10.1016/j.precamres.2013.12.022, 2014.

Bagas, L.: Early tectonic history of the Marymia Inlier and correlation with the Archaean Yilgarn Craton, Western Australia, Australian Journal of Earth Sciences, 46, 115-125, 10.1046/j.1440-0952.1999.00691.x, 1999.

640   Betts, P., Williams, H., Stewart, J., and Ailleres, L.: Kinematic analysis of aeromagnetic data: Looking at geophysical data in a structural context, Gondwana Research, 11, 582-583, 2007.

Betts, P. G., Valenta, R. K., and Finlay, J.: Evolution of the Mount Woods Inlier, northern Gawler Craton, Southern Australia: an integrated structural and aeromagnetic analysis, Tectonophysics, 366, 83-111, 2003.

Betts, P. G., Giles, D., and Lister, G. S.: Aeromagnetic patterns of half-graben and basin inversion: implications for sediment-hosted
645   massive sulfide Pb-Zn-Ag exploration, Journal of Structural Geology, 26, 1137-1156, 2004.

Blaikie, T. N., Ailleres, L., Cas, R. A. F., and Betts, P. G.: Three-dimensional potential field modelling of a multi-vent maar-diatreme — The Lake Coragulac maar, Newer Volcanics Province, south-eastern Australia, Journal of Volcanology and Geothermal Research, 235-236, 70-83, https://doi.org/10.1016/j.jvolgeores.2012.05.002, 2012.

Blaikie, T. N., Ailleres, L., Betts, P. G., and Cas, R. A. F.: A geophysical comparison of the diatremes of simple and complex maar
650   volcanoes, Newer Volcanics Province, south-eastern Australia, Journal of Volcanology and Geothermal Research, 276, 64-81, https://doi.org/10.1016/j.jvolgeores.2014.03.001, 2014.

Blewett, R. S., Czarnota, K., and Henson, P. A.: Structural-event framework for the eastern Yilgarn Craton, Western Australia, and its implications for orogenic gold, Precambrian Research, 183, 203-229, 10.1016/j.precamres.2010.04.004, 2010.

Braitenberg, C., Wienecke, S., Ebbing, J., Born, W., and Redfield, T.: Joint Gravity and Isostatic Analysis for Basement Studies–A Novel
655   Tool, 2007, 15-18,

Brethes, A., Guarnieri, P., Rasmussen, T. M., and Bauer, T. E.: Interpretation of aeromagnetic data in the Jameson Land Basin, central East Greenland: Structures and related mineralized systems, Tectonophysics, 724-725, 116-136, https://doi.org/10.1016/j.tecto.2018.01.008, 2018.

Briggs, I. C.: Machine contouring using minimum curvature, Geophysics, 39, 39-48, 1974.

660   Calcagno, P., Chilès, J. P., Courrioux, G., and Guillen, A.: Geological modelling from field data and geological knowledge: Part I. Modelling method coupling 3D potential-field interpolation and geological rules, Physics of the Earth and Planetary Interiors, 171, 147-157, 2008.

Clark, D. A.: Magnetic petrophysics and magnetic petrology: aids to geological interpretation of magnetic surveys, ASGO Journal of Australian Geology and Geophysics, 17, 83–103, 1997.

665   Cudahy, T. J., Jones, M., Thomas, M., Laukamp, C., Caccetta, M., Hewson, R., Rogdger, A., and Verrall, M.: Next generation mineral mapping: Queensland Airborne Hymap and Satellite ASTER Surveys 2006-2008. CSIRO report P2007/364, 153, 2008.

de Kemp, E., Jessell, M., Ailleres, L., Schetselaar, E., Hillier, M., Lindsay, M. D., and Brodaric, B.: Earth model construction in challenging geologic terrain: Designing workflows and algorithms that makes sense, Exploration 17: Sixth Decennial International Conference on Mineral Exploration, Toronto, 2017.

670   Deng, Y., Levandowski, W., and Kusky, T.: Lithospheric density structure beneath the Tarim basin and surroundings, northwestern China, from the joint inversion of gravity and topography, Earth and Planetary Science Letters, 460, 244-254, https://doi.org/10.1016/j.epsl.2016.10.051, 2017.

Dentith, M., Yuan, H., Murdie, R., Johnson, S., and Piña-Varas, P.: Application of deep-penetrating geophysical methods to mineral exploration: Examples from Western AustraliaDeep geophysics in mineral exploration, Geophysics, 83, WC29-WC41, 10.1190/geo2017-
675   0482.1, 2018.

Dufréchou, G., Harris, L. B., and Corriveau, L.: Tectonic reactivation of transverse basement structures in the Grenville orogen of SW Quebec, Canada: Insights from gravity and aeromagnetic data, Precambrian Research, 241, 61-84, https://doi.org/10.1016/j.precamres.2013.11.014, 2014.

Fairhead, J. D.: The structure of the lithosphere beneath the Eastern rift, East Africa, deduced from gravity studies, Tectonophysics, 30, 680 269-298, http://dx.doi.org/10.1016/0040-1951(76)90190-6, 1976.

Fullagar, P. K., Pears, G., Hutton, D., and Thompson, A.: 3D gravity and aeromagnetic inversion for MVT lead-zinc exploration at Pillara, Western Australia, Exploration Geophysics, 35, 142-146, doi:10.1071/EG04142, 2004.

Giraud, J., Lindsay, M., Ogarko, V., Jessell, M., Martin, R., and Pakyuz-Charrier, E.: Integration of geoscientific uncertainty into geophysical inversion by means of local gradient regularization, Solid Earth, 10, 193-210, 10.5194/se-10-193-2019, 2019.

685 Grant, F. S.: Aeromagnetics, geology and ore environments, I. Magnetite in igneous, sedimentary and metamorphic rocks: An overview, Geoexploration, 23, 303-333, 10.1016/0016-7142(85)90001-8, 1985.

Guillen, A., Calcagno, P., Courrioux, G., Joly, A., and Ledru, P.: Geological modelling from field data and geological knowledge: Part II. Modelling validation using gravity and magnetic data inversion, Physics of the Earth and Planetary Interiors, 171, 158-169, 2008.

Gunn, P. J.: Quantitative methods for interpreting aeromagnetic data: a subjective review, AGSO Journal of Australian Geology and 690 Geophysics, 17, 105-114, 1997.

Hackney, R.: Gravity anomalies, crustal structure and isostasy associated with the Proterozoic Capricorn Orogen, Western Australia, Precambrian Research, 128, 219-236, http://dx.doi.org/10.1016/j.precamres.2003.09.012, 2004.

Hawke, M. L., Meffre, S., Stein, H., Hilliard, P., Large, R., and Gemmell, J. B.: Geochronology of the DeGrussa volcanic-hosted massive sulphide deposit and associated mineralisation of the Yerrida, Bryah and Padbury Basins, Western Australia, Precambrian Research, 267, 695 250-284, http://dx.doi.org/10.1016/j.precamres.2015.06.011, 2015.

Hawke, M. L.: The Geological Evolution of the DeGrussa volcanic-hosted massive sulfide deposit and the Eastern Capricorn Orogen, Western Australia, PhD, Centre for Ore Deposit and Earth Sciences, School of Physical Sciences, The University of Tasmania, Hobart, Tasmania, 434 pp., 2016.

Heinson, G. S., Direen, N. G., and Gill, R. M.: Magnetotelluric evidence for a deep-crustal mineralizing system beneath the Olympic Dam 700 iron oxide copper-gold deposit, southern Australia, Geology, 34, 573-576, 10.1130/G22222.1, 2006.

Hildenbrand, T. G., Berger, B., Jachens, R. C., and Ludington, S.: Regional Crustal Structures and Their Relationship to the Distribution of Ore Deposits in the Western United States, Based on Magnetic and Gravity Data, Economic Geology, 95, 1583-1603, 10.2113/95.8.1583, 2000.

Husson, E., Guillen, A., Séranne, M., Courrioux, G., and Couëffé, R.: 3D Geological modelling and gravity inversion of a structurally 705 complex carbonate area: application for karstified massif localization, Basin Research, 30, 766-782, 10.1111/bre.12279, 2018.

Jessell, M.: Noddy - an interactive map creation package, MSc, University of London, 52 pp., 1981.

Jessell, M., Aillères, L., de Kemp, E., Lindsay, M., Wellmann, F., Hillier, M., Laurent, G., Carmichael, T., and Martin, R.: Next Generation Three-Dimensional Geologic Modeling and Inversion, Society of Economic Geologists: Special Publication 18, 261-272, 2014.

710 Jessell, M. W., and Valenta, R. K.: Structural geophysics: Integrated structural and geophysical modelling, in: Computer Methods in the Geosciences, edited by: Declan, G. D. P., Pergamon, 303-324, 1996.

Jessell, M. W., Begg, G. C., and Miller, M. S.: The geophysical signatures of the West African Craton, Precambrian Research, 274, 3-24, https://doi.org/10.1016/j.precamres.2015.08.010, 2016.

Johnston, D. T., Poulton, S. W., Fralick, P. W., Wing, B., Canfield, D. E., and Farquhar, J.: Evolution of the oceanic sulfur cycle at the end 715 of the Paleoproterozoic, Geochimica et Cosmochimica Acta, 70, 5723-5739, 2006.

Kohanpour, F., Lindsay, M. D., Occhipinti, S., and Gorczyk, W.: Structural controls on proterozoic nickel and gold mineral systems identified from geodynamic modelling and geophysical interpretation, east Kimberley, Western Australia, Ore Geology Reviews, 95, 552-568, https://doi.org/10.1016/j.oregeorev.2018.03.010, 2018.

Kovesi, P.: Phase Preserving Tone Mapping of Non-Photographic High Dynamic Range Images, 2012 International Conference on Digital 720 Image Computing Techniques and Applications (DICTA), 2012, 1-8,

LaFlamme, C., Fiorentini, M. L., Lindsay, M. D., and Bui, T. H.: Atmospheric sulfur is recycled to the crystalline continental crust during supercontinent formation, Nature Communications, 9, 4380, 10.1038/s41467-018-06691-3, 2018.

LaFlamme, C., Fiorentini, M., and Beaudoin, B. C.: Insight into the seawater sulfate reservoir at 2.0 Ga from the Paleoproterozoic Degrussa Cu-Au volcanogenic massive sulfide deposit, Geochimica et Cosmochimica Acta, In review.

725 Lindsay, M. D., Aillères, L., Jessell, M. W., de Kemp, E. A., and Betts, P. G.: Locating and quantifying geological uncertainty in three-dimensional models: Analysis of the Gippsland Basin, southeastern Australia, Tectonophysics, 546–547, 10-27, 10.1016/j.tecto.2012.04.007, 2012.

Lindsay, M. D., Occhipinti, S., Aitken, A. R. A., Metelka, V., Hollis, J., and Tyler, I.: Proterozoic accretionary tectonics in the east Kimberley region, Australia, Precambrian Research, 278, 265-282, http://dx.doi.org/10.1016/j.precamres.2016.03.019, 2016.

730 Lindsay, M. D., Spratt, J., Occhipinti, S. A., Aitken, A. R. A., Dentith, M. C., Hollis, J. A., and Tyler, I. M.: Identifying mineral prospectivity using 3D magnetotelluric, potential field and geological data in the east Kimberley, Australia, Geological Society, London, Special Publications, 453, 10.1144/sp453.8, 2017.

Manger, G. E.: Porosity and bulk density of sedimentary rocks: Contributions to geochemistry, Geological Survey Bulletin, 1144-E, E1-E55, 1963.

735 Mueller, D. H. A.: Final report on drilling of THD001: a 1017.8 m vertical core hole on E52/1673: GSWA reference C144/2005, Sipa Exploration NL, 2011.

Müller, D., and Groves, D. I.: Implications for Mineral Exploration in Arc Environments, in: Potassic Igneous Rocks and Associated Gold-Copper Mineralization, edited by: Müller, D., and Groves, D. I., Springer International Publishing, Cham, 337-354, 2019.

Nettleton, L. L.: Gravity and magnetic calculations, Geophysics, 7, 293-310, 1942.

740 Occhipinti, S., Hocking, R., Lindsay, M., Aitken, A., Copp, I., Jones, J., Sheppard, S., Pirajno, F., and Metelka, V.: Paleoproterozoic basin development on the northern Yilgarn Craton, Western Australia, Precambrian Research, 300, 121-140, http://dx.doi.org/10.1016/j.precamres.2017.08.003, 2017.

Occhipinti, S. A., Grey, K., Pirajno, F., Adamides, N. G., Bagas, L., Dawes, P., and Le Blanc-Smith, G.: Stratigraphic revision of the Palaeoproterozoic rocks of the Yerrida, Bryah and Padbury Basins (formerly Glengarry Basin), 1997.

745 Olierook, H. K. H., Sheppard, S., Johnson, S. P., Occhipinti, S. A., Reddy, S. M., Clark, C., Fletcher, I. R., Rasmussen, B., Zi, J.-W., Pirajno, F., LaFlamme, C., Do, T., Ware, B., Blandthorn, E., Lindsay, M., Lu, Y.-J., Crossley, R. J., and Erickson, T. M.: Extensional episodes in the Paleoproterozoic Capricorn Orogen, Western Australia, revealed by petrogenesis and geochronology of mafic–ultramafic rocks, Precambrian Research, 306, 22-40, https://doi.org/10.1016/j.precamres.2017.12.015, 2018.

Pearce, J. A.: Geochemical fingerprinting of oceanic basalts with applications to ophiolite classification and the search for Archean 750 oceanic crust, Lithos, 100, 14-48, https://doi.org/10.1016/j.lithos.2007.06.016, 2008.

Pearce, J. A.: Immobile Element Fingerprinting of Ophiolites, Elements, 10, 101-108, 10.2113/gselements.10.2.101, 2014.

Perrouty, S., Aillères, L., Jessell, M. W., Baratoux, L., Bourassa, Y., and Crawford, B.: Revised Eburnean geodynamic evolution of the gold-rich southern Ashanti Belt, Ghana, with new field and geophysical evidence of pre-Tarkwaian deformations, Precambrian Research, 204-205, 12-39, 2012.

755 Perrouty, S., Gaillard, N., Piette-Lauzière, N., Mir, R., Bardoux, M., Olivo, G. R., Linnen, R. L., Bérubé, C. L., Lypaczewski, P., Guilmette, C., Feltrin, L., and Morris, W. A.: Structural setting for Canadian Malartic style of gold mineralization in the Pontiac Subprovince, south of the Cadillac Larder Lake Deformation Zone, Québec, Canada, Ore Geology Reviews, 84, 185-201, https://doi.org/10.1016/j.oregeorev.2017.01.009, 2017.

Perrouty, S., Linnen, R. L., Lesher, C. M., Olivo, G. R., Piercey, S. J., Gaillard, N., Clark, J. R., and Enkin, R. J.: Expanding the size of 760 multi-parameter metasomatic footprints in gold exploration: utilization of mafic dykes in the Canadian Malartic district, Québec, Canada, Mineralium Deposita, 10.1007/s00126-018-0829-x, 2018.

Pirajno, F., and Occhipinti, S. A.: Geology of the Bryah 1:100 00 sheet, Geological Survey of Western Australia, 1998.

Pirajno, F., Occhipinti, S. A., and Swager, C. P.: Geology and tectonic evolution of the Palaeoproterozoic Bryah, Padbury and Yerrida basins (formerly Glengarry Basin), Western Australia: implications for the history of the south-central Capricorn Orogen, Precambrian 765 Research, 90, 119-140, 10.1016/S0301-9268(98)00045-X, 1998.

Pirajno, F., and Occhipinti, S. A.: Three Palaeoproterozoic basins-Yerrida, Bryah and Padbury-Capricorn Orogen, Western Australia, Australian Journal of Earth Sciences, 47, 675-688, 10.1046/j.1440-0952.2000.00800.x, 2000.

Quigley, M. C., Bennetts, L. G., Durance, P., Kuhnert, P. M., Lindsay, M. D., Pembleton, K. G., Roberts, M. E., and White, C. J.: The provision and utility of science and uncertainty to decision-makers: earth science case studies, Environment Systems and Decisions, 770   10.1007/s10669-019-09728-0, 2019.

Reichelt, R.: Géologie du Gourma (Afrique occidentale), un seuil et un bassin du Précambrien supérieur, Mém. BRGM, no 53, 1971.

Sanchez-Rojas, J., and Palma, M.: Crustal density structure in northwestern South America derived from analysis and 3-D modeling of gravity and seismicity data, Tectonophysics, 634, 97-115, https://doi.org/10.1016/j.tecto.2014.07.026, 2014.

Sun, S.-s., and McDonough, W. F.: Chemical and isotopic systematics of oceanic basalts: implications for mantle composition and 775   processes, Geological Society, London, Special Publications, 42, 313-345, 10.1144/gsl.Sp.1989.042.01.19, 1989.

Talwani, M., Worzel, J. I., and Landisman, M.: Rapid gravity computations for twodimensional bodies with application to the Mendicino submarine fracture zone, Journal of Geophysical Research, 64, 49-59, 1959.

Talwani, M., and Heirtzler, J. R.: Computation of magnetic anomalies caused by two-dimensional bodies of arbitrary shape, in: Computers in the Mineral Industries, edited by: Parks, G. A., School of Earth Sciences, Stanford University, 464-480, 1964.

780   Tarantola, A.: Popper, Bayes and the inverse problem, Nat Phys, 2, 492-494, 2006.

Telford, W. M., Geldart, L. P., and Sheriff, R. E.: Applied Geophysics, 2nd ed., Cambridge University Press, Cambridge, UK, 1990.
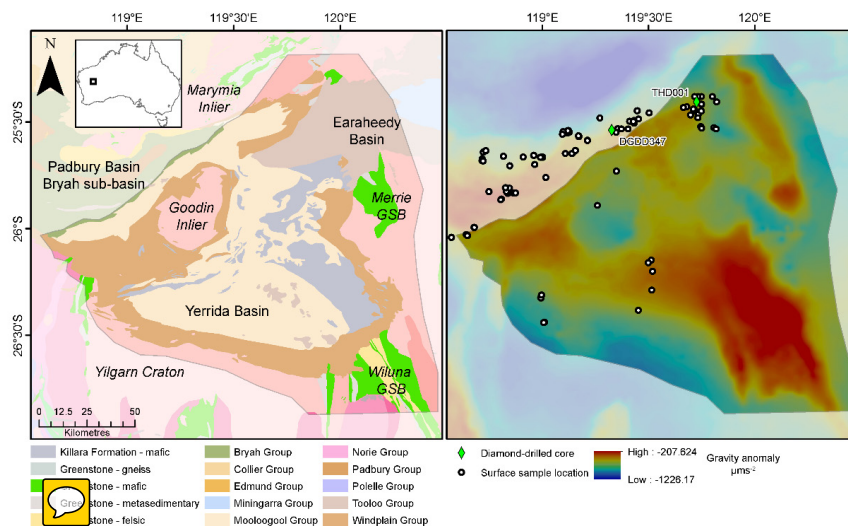
785 **Figure 1. Location and geology of the Yerrida Basin, Capricorn Orogen (left). Bouguer gravity image of the Yerrida Basin shown with sampling locations for petrophysical and geochemical data. Points represent surface sample locations; diamonds represent location of diamond-drilled core collars with name. Significant regions are labelled, with Archean rocks shown with italic font. GSB = greenstone belt.**
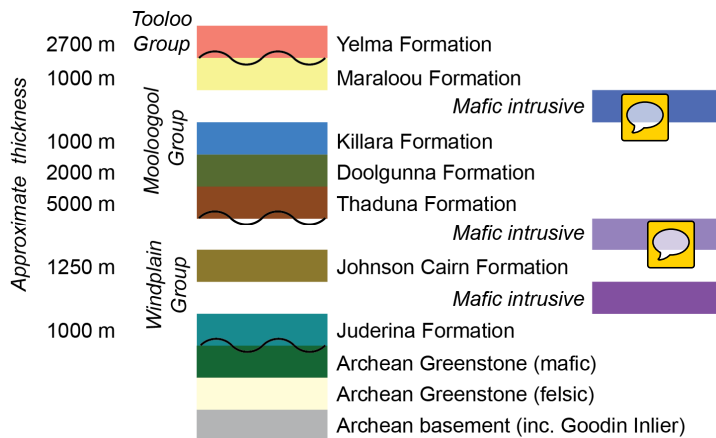
790 **Figure 2. Stratigraphy and input for the Yerrida Basin 3D model modified from Occhipinti et al. (2017). The position of unconformities are indicated with a wavy line and approximate thickness are given. The position of the mafic intrusives are shown to indicate the possible stratigraphic position being tested by geophysical modelling.**
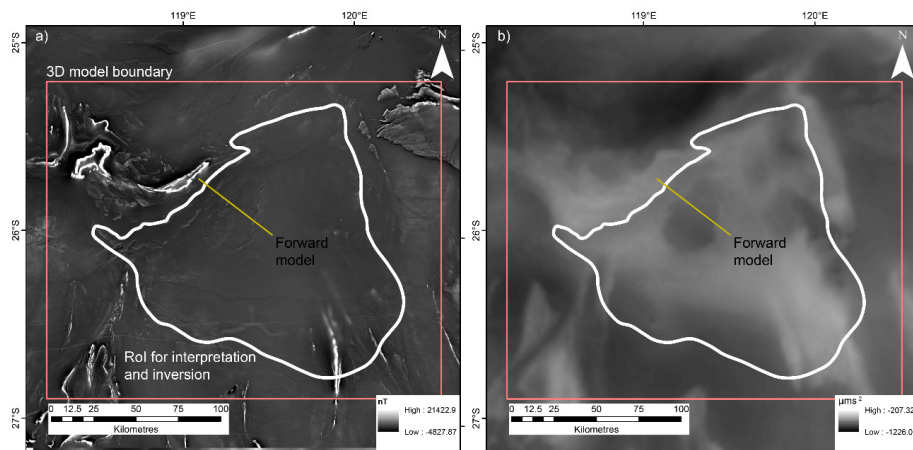
Figure 3. Geophysical grids and forward model location trace (as indicated). a) Magnetic anomaly and b) Bouguer gravity anomaly.
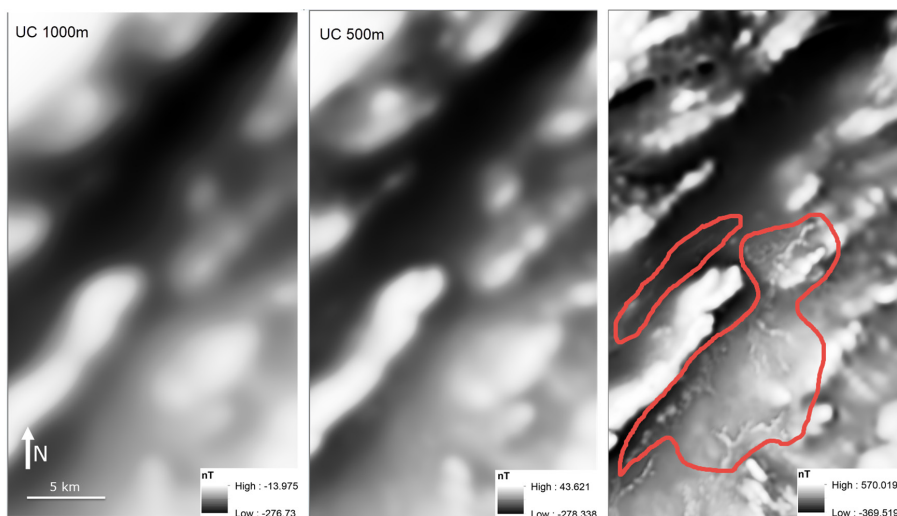
Figure 4. In order to view non-regolith rock units, upward continuation was performed on RTP magnetic data to filter short wavelength magnetic anomalies attributed to surficial stream sediments and other forms of regolith. Upward continuation of 1000 m (left); 500 m (right) and the original, unfiltered RTP magnetic data. Examples of the types of anomaly that were targeted for filtering are circled in red. Such anomalies of surficial transported regolith add noise to a geophysical interpretation and increase the likelihood of misinterpretation of structure. Location is centred on 119.162 E – 25.908 S.
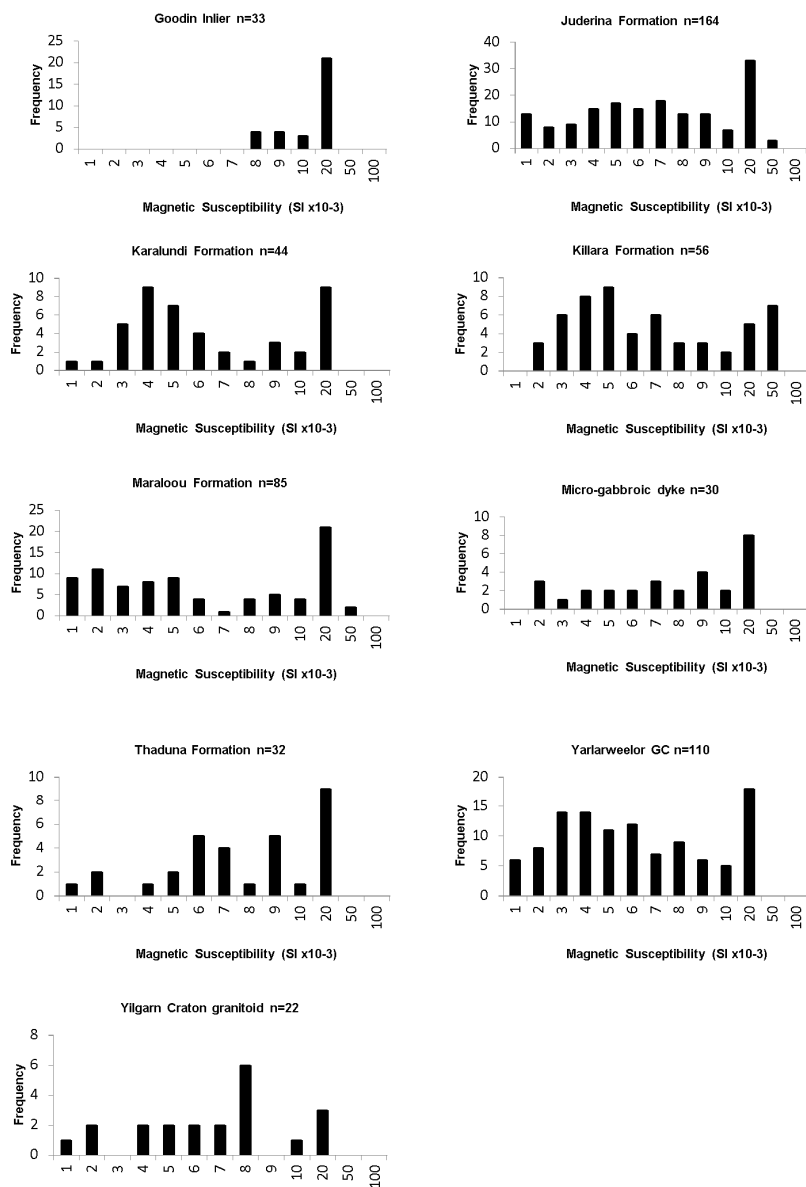
Figure 5. Histogram representation of measured magnetic susceptibility from Yerrida Basin rocks.

805
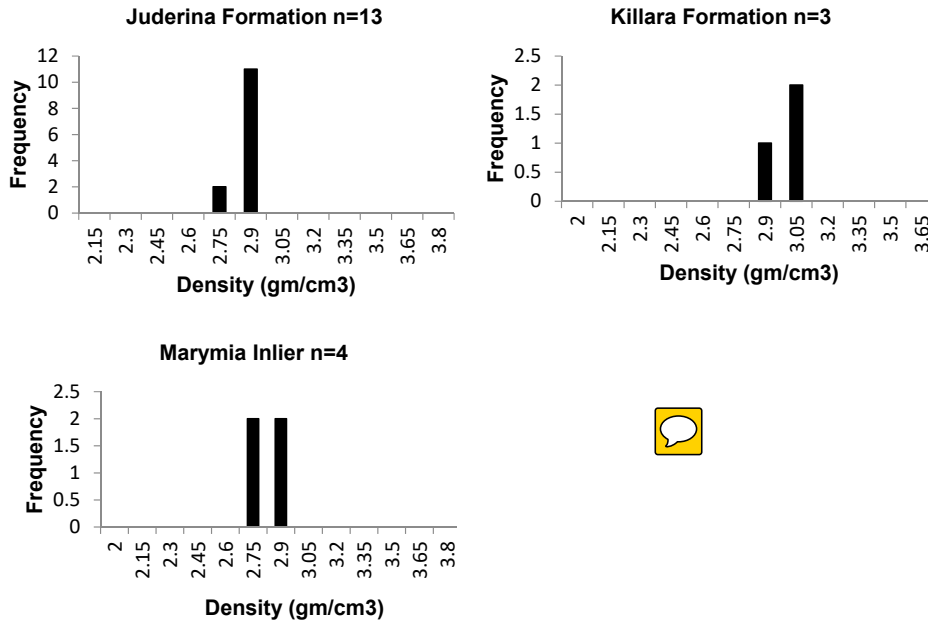
Figure 6. Histogram representation of measured Archimedes bulk density of Yerrida Basin rocks
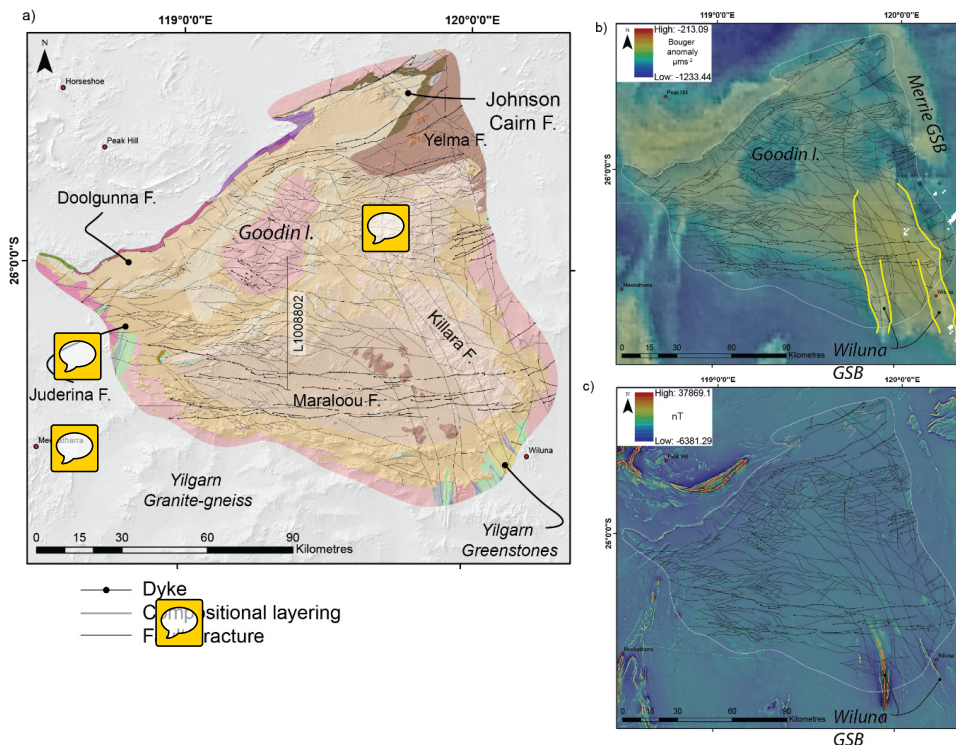
810

Figure 7. Structural geophysical interpretation of the southern Yerrida Basin. (a) Integrated interpretation of structure and rock units. The location of AEM line L1008802 is shown – refer Figure 8a. (b) Interpreted structure shown with gravity data (blended image: Bouguer anomaly shown in colour with 1VD of the Bouguer anomaly in greyscale). (c) Interpreted structure shown with blended magnetic data (blended image: RTP shown in colour with 1VD of the RTP shown in greyscale). GSB = greenstone belt.
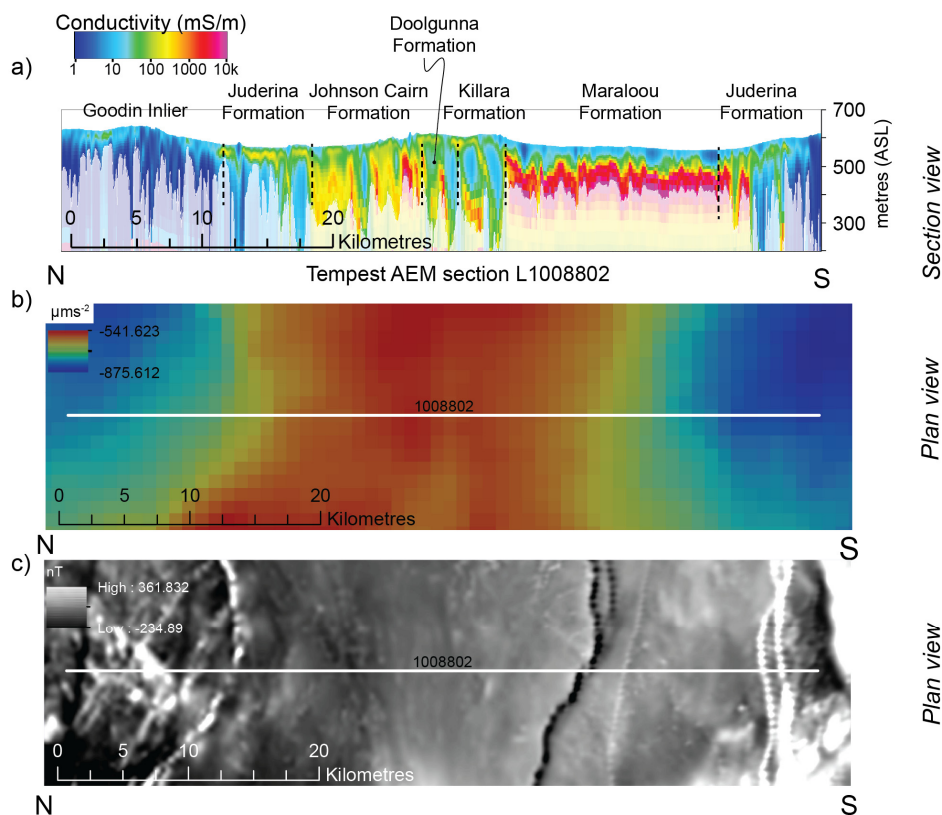
Figure 8. Airborne electromagnetic data (AEM) and lithological interpretation. AEM data was useful to distinguish lithologies to support the overall interpretation. a) Tempest AEM section L1008802 labelled with formations correlated to the surface geology maps (see Figure 7a for location). b) Plan view of the gravity grid at the same location. The lower resolution of this data proved less useful the AEM for lithological interpretation at this scale. c) Plan view of magnetic data at the same location. While higher resolution than the gravity data, lithological interpretation is more difficult compared to the imaging provide by AEM data.

815
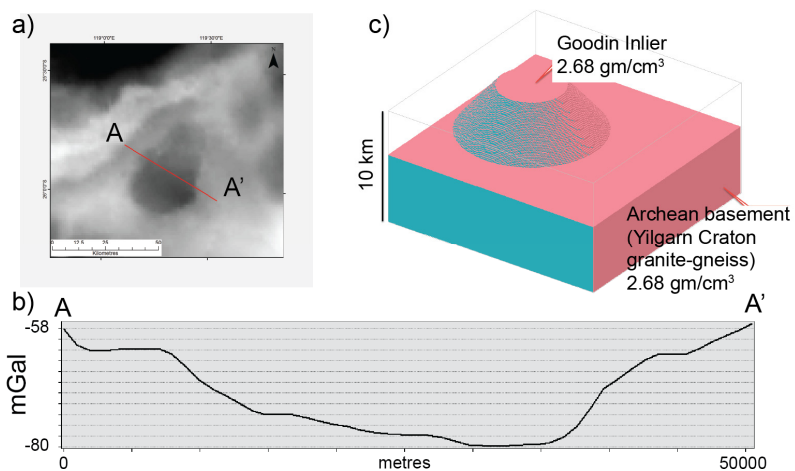
820

825
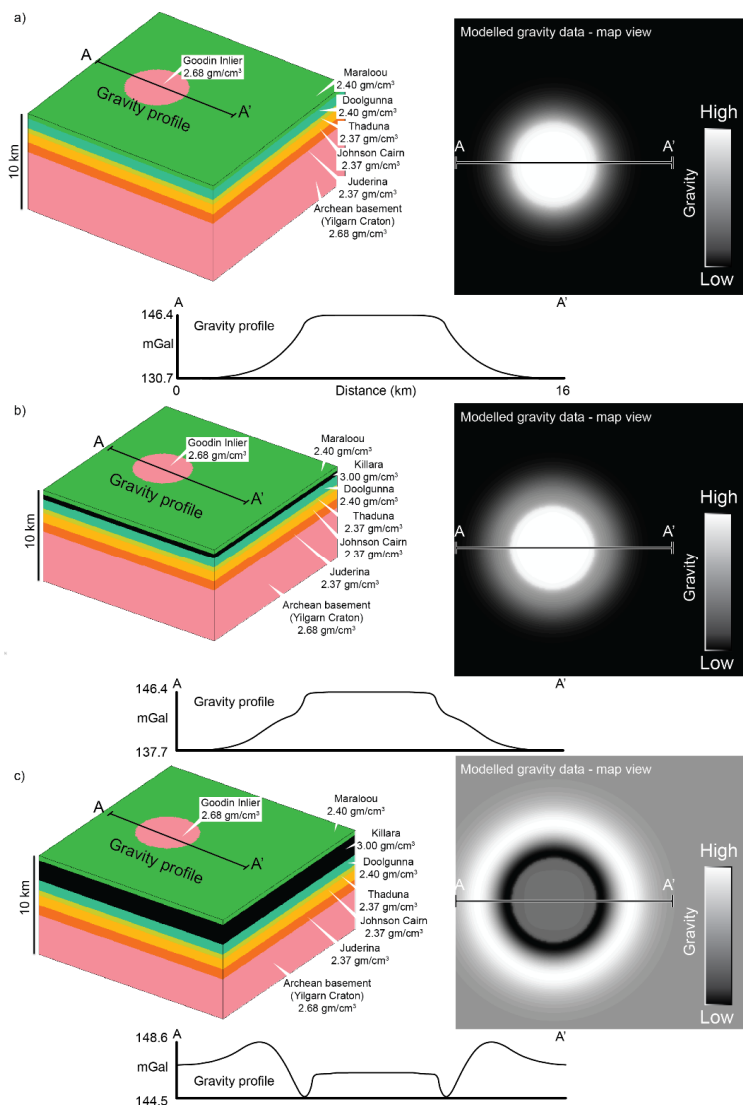
Figure 10. Conceptual forward modelling results obtained from Noddy. (a) No Killara formation; (b) 500 m of Killara Formation and (c) 2000 m of Killara Formation.
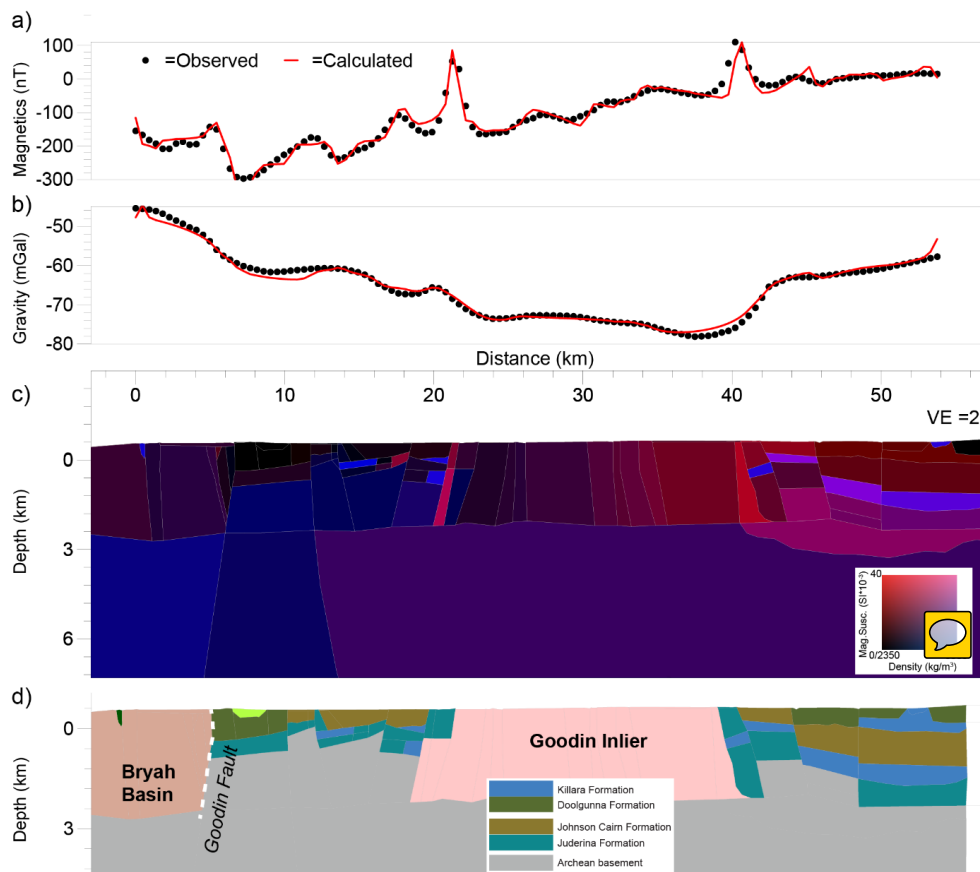
830 **Figure 11. Section-based forward modelling of the Yerrida Basin and Goodin Inlier – location of profile shown in Figure 2. The top two panels show the degree of fit between the observed (points) and calculated (line) geophysical response for magnetic (a) and gravity (b) data. The middle panel (c) shows the petrophysical model that was used to model the calculated geophysical response. The bottom panel (d) shows the geological interpretation made from the petrophysical model.**
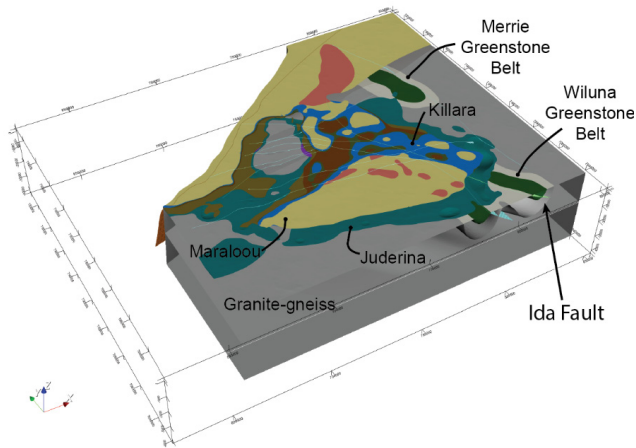
835   **Figure 12: 3D model constructed to constrain geophysical inversion. Oblique view from SW - check marks on the X-axis are at 50 km intervals; Y-axis at 20 km intervals; Z-axis 10 km.**
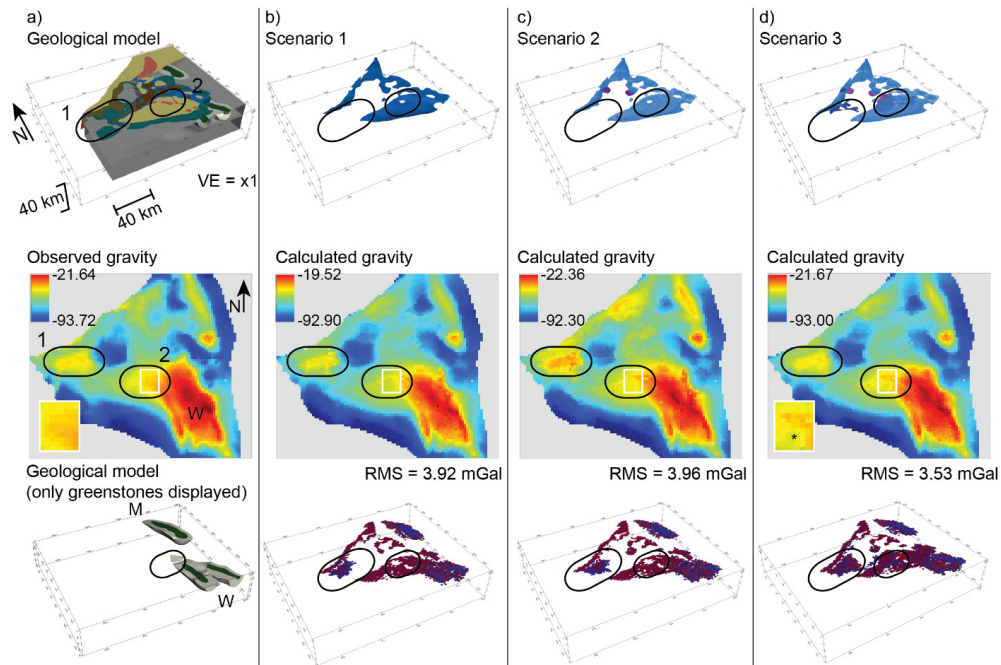
Figure 13. Geological models and mafic intrusive scenarios subjected to inversion modelling. a) Top panel: 3D geological model; middle panel – observed gravity response; bottom panel - location of greenstone belts. b-d) Results from scenarios 1-3 respectively: top – position of mafic intrusions; middle - calculated gravity response; bottom – distribution of locations determined by the inversion to be >2.9 gms/cm3. Colours in the gravity response indicate blue = low; yellow = moderate; red = high. Check marks on the X-axis are at 50 km intervals; Y-axis at 20 km intervals; Z-axis 10 km.
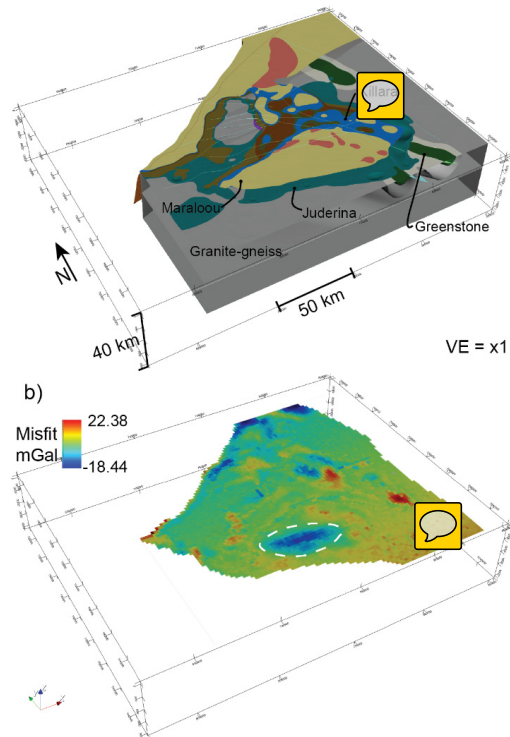
Figure 14. Assessing the plausibility of the Yerrida Basin model with geological knowledge and geophysical inversion. a) The 3D model representing scenario 3 and b) the remaining misfit between the inverted geological model and geophysical data. Misfit is shown after regional trend effects have been removed using a linear solver. Red = density exceeds that required by observed gravity, blue = density lower than that required by observed gravity. Note the large region of misfit outlined by the white dashed line that indicates the position of where a portion of material needs to be removed to result in reduced misfit. The cause of this misfit is considered to be due to the modelled basin rocks being too thick. Check marks on the X-axis are at 50 km intervals; Y-axis at 20 km intervals; Z-axis 10 km.
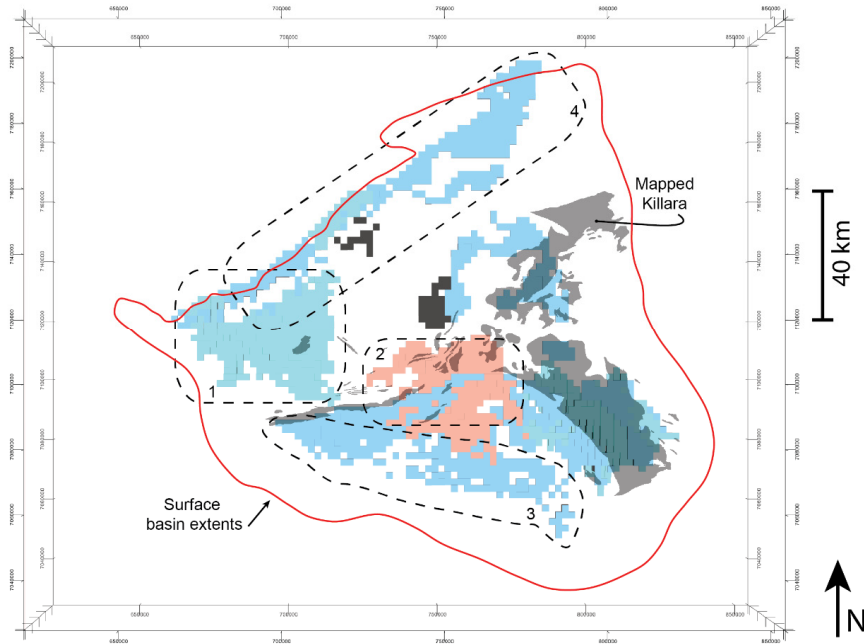
Figure 15. Comparison of mafic units at depth with mapped Killara Formation. Mafic units are colour-coded to help differentiate bodies added during scenario testing. Check marks on the X-axis are at 50 km intervals; Y-axis at 20 km intervals; Z-axis 10 km.
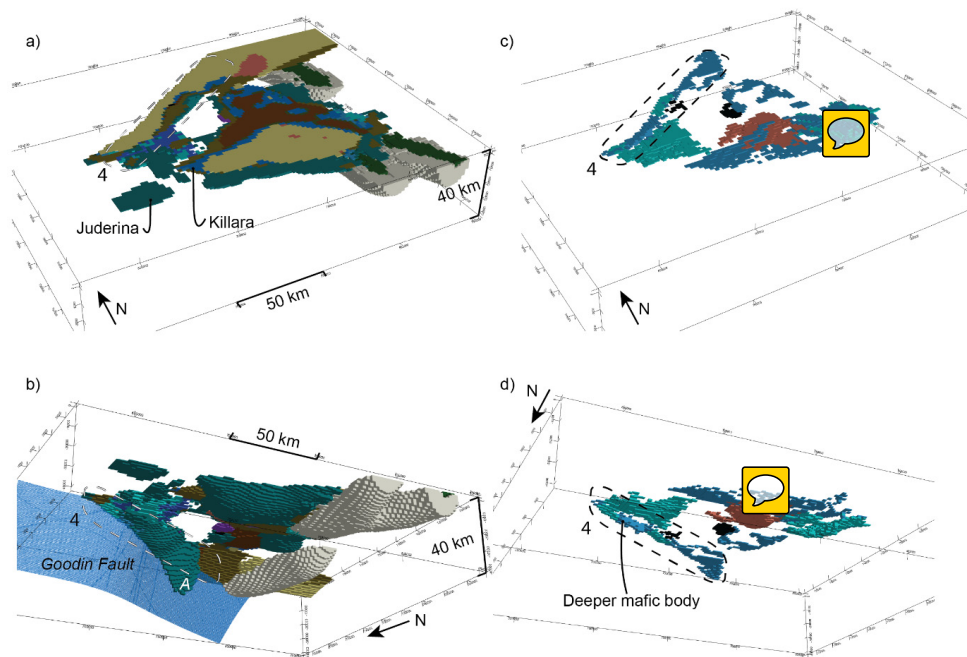
Figure 16. 3D model showing distribution of high density (>2.9 gms/cm3) material: a) – d) show different views of the model, with regions discussed in-text labelled accordingly. Check marks on the X-axis are at 50 km intervals; Y-axis at 20 km intervals; Z-axis 10 km.
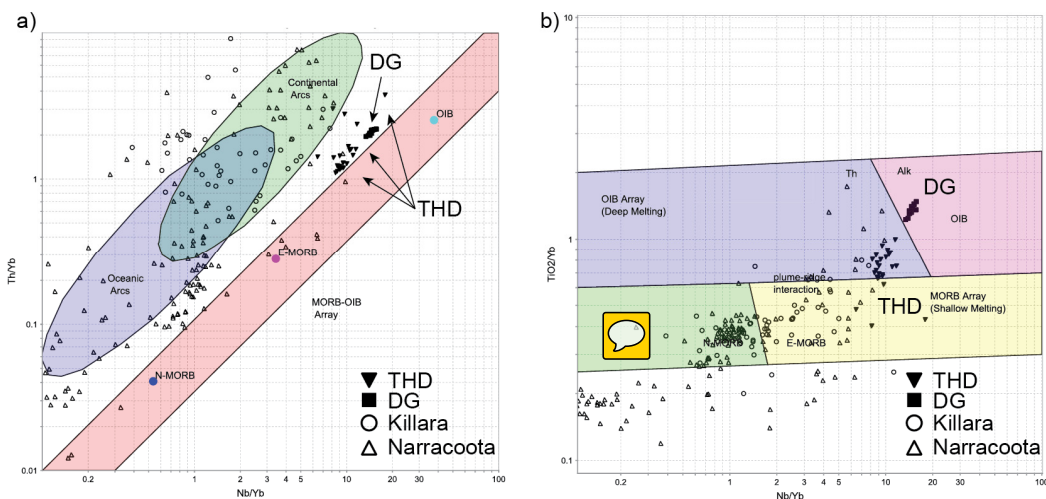
Figure 17. a) Discriminant basalt Th/Yb vs Nb/Yb diagram of mafic geochemistry from the Yerrida Basin and b) discriminant
860 **Nb/Yb and TiO₂/Yb diagram. Data compiled from Olierook et al. (2018) and ,**
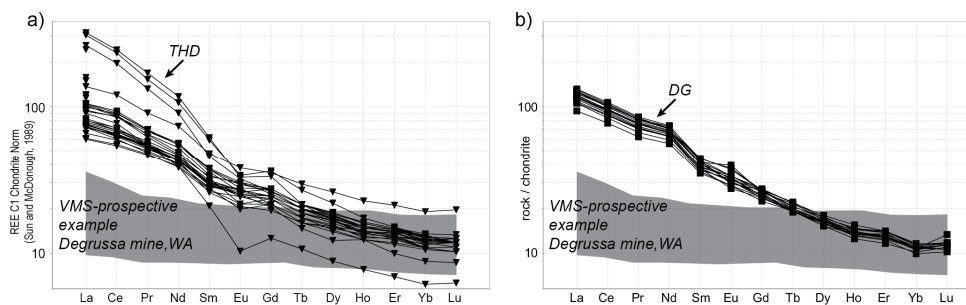
Figure 18. REE spider diagrams for mafic rocks sampled from a) THD001 and b) DDGD347. Note the inclined profiles for each indicated a non-prospective environment for VMS mineralisation. The shaded portion indicates a VMS-prospective example taken from basaltic and micro-gabbroic rocks sampled from the Degrussa mine (Hawke, 2016).
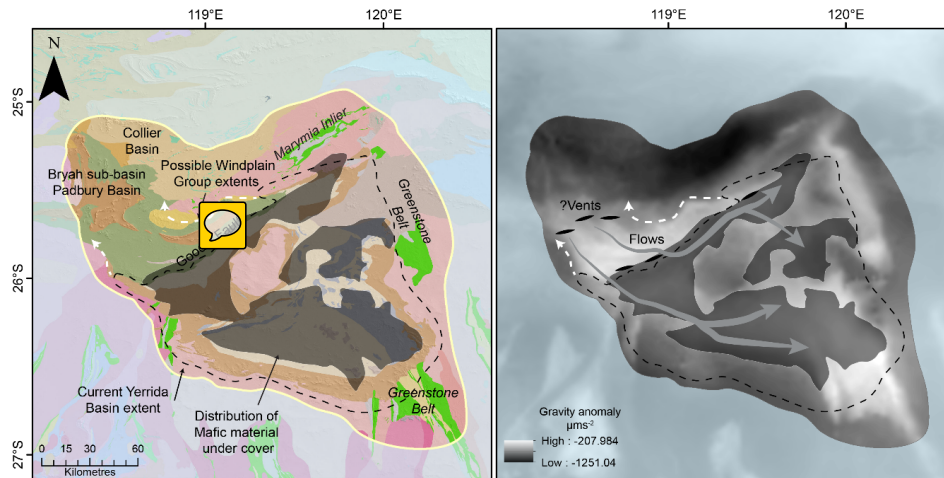
865

Figure 19. Proposed source of magmatism for the mafic component of the Yerrida Basin. The lack of an Archean signature in the mafic rocks suggests that conduits for magmatism do not include the Yilgarn Craton rocks that underlie the Yerrida Basin, but likely sourced from the northeast or along the current position of the Goodin Fault. a) Major components of the southern Capricorn region are shown, with Archean regions listed in italics. Shaded regions show the position of mafic material determined
870 **via geophysical inversion. b) Vent locations and flow or sill intrusion paths are proposed and shown over the Bouguer gravity anomaly.**

Table 1. Petrophysical statistics calculated from rock sample measurements.

Magnetic Susceptibilty			
Formation / Rock type	*Sample size (n)*	*Mean (SI×10^{-3})*	*Std. dev. (SI×10$^{-3)}$*
Dyke	30	6.20	4.26
Goodin Inlier	33	10.31	2.06
Juderina	164	5.04	4.16
Karalundi	44	5.14	2.62
Killara	56	5.74	6.16
Maraloou	85	4.76	3.83
Narracoota	127	3.36	2.58
Yilgarn Craton granitoid	22	5.54	3.63
Thaduna	32	6.66	5.19
Density			
		Mean (gm/cm^3)	*Std. dev. (gm/cm^3)*
Goodin Inlier	1	2.68	NA
Juderina	13	2.82	0.055
Killara	3	2.89	0.111
Marymia Inlier	4	2.73	0.086
Yilgarn Craton grantoid	2	2.68	0.029
Thaduna	1	2.40	NA